Selective sweeps influence diversity over large regions of the mouse genome

Tom R. Booker[1,2], Benjamin C. Jackson[3], Rory J. Craig[3], Brian Charlesworth[3], Peter D. Keightley[3]

1. Department of Zoology, University of British Columbia, Vancouver, British Columbia, Canada.
2. Department of Biological Sciences, University of Calgary, Calgary, Alberta, Canada.
3. Institute of Evolutionary Biology, University of Edinburgh, Edinburgh, UK. EH9 3FL

Correspondence: booker@zoology.ubc.ca

Abstract

To what extent do substitutions in protein-coding versus gene-regulatory regions contribute to fitness change over time? Answering this question requires estimates of the extent of selection acting on beneficial mutations in the two classes of sites. New mutations that have advantageous or deleterious fitness effects can induce selective sweeps and background selection, respectively, causing variation in the level of neutral genetic diversity along the genome. In this study, we analyse the profiles of genetic variability around protein-coding and regulatory elements in the genomes of wild mice to estimate the parameters of positive selection. We find patterns of diversity consistent with the effects of selection at linked sites, which are similar across mouse taxa, despite differences in effective population size and demographic history. By fitting a model that combines the effects of selective sweeps and background selection, we estimate the strength of positive selection and the frequency of advantageous mutations. We find that strong positive selection is required to explain variation in genetic diversity across the murid genome. In particular, we estimate that beneficial mutations in protein-coding regions have stronger effects on fitness than do mutations in gene-regulatory regions, but that mutations in gene-regulatory regions are more common. Overall though, our parameter estimates suggest that the cumulative fitness changes brought about by beneficial mutations in protein-coding may be greater than those in gene-regulatory elements.

Introductions

Understanding the relative contributions of protein-coding and gene regulatory variation to adaptation is a long-standing goal of evolutionary biology. Molecular changes in protein-coding and gene regulatory regions contribute to evolution, but in classic essays King and Wilson (1975) and Carroll (2005) argued that changes in gene expression may dominate adaptive evolution. King and Wilson (1975) reasoned that since nucleotide identity between human and chimpanzee proteins is around 99%, there are too few protein sequence difference between the species, implying that changes in gene regulation are probably required to explain the many phenotypic differences between the species. Carroll's (2005) argument highlighted the idea that molecular changes in the gene regulatory apparatus may have smaller pleiotropic effects than those in protein-coding regions, so that changes in gene expression may dominate adaptive evolution. However, Hoekstra and Coyne (2007) attempted to refute these arguments, maintaining that there is insufficient evidence to decide whether adaptation is primarily driven by changes in protein sequences or gene regulatory elements. For example, a 1% difference in protein sequence between humans and chimpanzees could still result in a very large number of phenotypic differences. However, the contribution of individual variants to additive genetic variance for a trait is expected to be proportional to the square of their phenotypic effect sizes, assuming semi-dominance (Fisher 1918; Falconer and Mackay 1996). Without an understanding of the frequencies of new mutations, their effect sizes, and the strength of selection acting on them, the question of the contribution of molecular evolution in different genomic elements to adaptation will remain intractable.

Information on the strength of selection acting on beneficial mutations and the rates at which they occur can be obtained by analysing patterns of neutral genetic diversity. Because genetically linked sites do not evolve independently, natural selection acting at a given site may leave signatures at linked sites that are informative about the strength and mode of selection. The effects of selection at linked sites on neutral genetic diversity depend on the frequency and strength of selected mutations and the rate of recombination (Charlesworth 2012; Hermisson and Pennings 2017; Stephan 2019). Several modes of selection at linked sites have been identified. Of specific relevance to this study are background selection (BGS), caused by the removal of deleterious mutations from a population, and selective sweeps, caused by the spread of advantageous variants. The classic footprint of a selective sweep is a trough in nucleotide diversity

67 at neutral sites surrounding an adaptive substitution. The reduction in nucleotide diversity caused
68 by a sweep is proportional to the ratio of the strength of selection acting on the causal mutation
69 to the local recombination rate (Barton 2000). Using such information, Wiehe and Stephan (1993)
70 developed a model of recurrent selective sweeps and used it to estimate the frequency and
71 strength of advantageous mutations in *Drosophila melanogaster*. They fitted their model of
72 sweeps to the relationship between recombination rate and nucleotide diversity for a number of
73 loci sampled across the *D. melanogaster* genome. At the time of their analysis, the theory of BGS
74 was in its infancy, and models combining the effects of BGS and sweeps had not been developed.
75 However, the effects of BGS are expected to be ubiquitous across the genome (McVicker et al.
76 2009; Comeron, 2014; Elyashiv et al. 2016; Pouyet et al. 2018), and conceptually similar studies to
77 Wiehe and Stephan (1993) have shown that controlling for BGS is important when parametrizing
78 sweep models (Kim and Stephan 2000; Comeron 2014; Elyashiv et al. 2016; Campos et al. 2017).
79
80 In *Drosophila*, there are reductions in average diversity around recent nonsynonymous
81 substitutions, which are greater than those observed around synonymous substitutions (Sattath et
82 al. 2011; Elyashiv et al. 2016). To investigate the causes of this difference, Elyashiv et al. (2016)
83 fitted a model of sweeps and BGS to genome-wide variation in genetic diversity in *D.*
84 *melanogaster* and found that a combination of BGS and selective sweeps provided a close fit to
85 the observed data. From the fit of their model to empirical data, Elyashiv et al. (2016) inferred a
86 distribution of fitness effects for advantageous mutations that included a class of very strongly
87 selected mutations and a more mildly beneficial class. In both mice and humans, however, there is
88 very little difference between the profiles of diversity around recent nonsynonymous and
89 synonymous substitutions (Hernandez et al. 2011; Halligan et al. 2013). In these species, dips in
90 average nucleotide diversity have been observed in genomic regions surrounding whole functional
91 elements, such as protein-coding exons or conserved non-coding elements, which may reflect the
92 cumulative effects of recurrent selective sweeps and BGS (Hernandez et al. 2011; Halligan et al.
93 2013; Booker and Keightley 2018)
94
95 Natural populations of mice in the genus *Mus* are excellent material for the study of adaptive
96 evolution in different regions of the mammalian genome. Their populations are very large
97 compared to other mammals (Leffler et al. 2012), so there is likely to be more power for
98 population genetic analyses to differentiate between the evolutionary processes that affect
99 genetic variability. Previous studies in mice have established that both protein-coding genes and

100 regions putatively involved in gene regulation have an excess of sequence differences from sister
101 taxa compared to that expected under a model of purifying selection, suggesting widespread
102 adaptive molecular evolution (Halligan et al. 2010, 2013). Halligan et al. (2013) analysed a sample
103 of *Mus musculus castaneus* individuals and estimated that there have been around 1.3 million and
104 0.38 million positively selected regulatory and nonsynonymous changes, respectively, over the
105 period since this subspecies began to diverge from rats. At face value, this finding suggests that
106 changes in gene regulation may dominate adaptive evolution in mice. However, Halligan et al.
107 (2013) also showed that there are much larger reductions in neutral diversity surrounding protein-
108 coding exons than around gene regulatory elements, and that BGS could not fully explain these
109 observations (Halligan et al. 2013; Booker and Keightley 2018). Halligan et al. (2013) concluded
110 that this difference in neutral diversity may reflect differences in the strength of positive selection
111 acting on the different classes of sites.
112
113 Building on Halligan et al. (2013), we have sought to tease apart the contributions of BGS and
114 sweeps to the patterns of nucleotide diversity observed in the Eastern house mouse *M. m.*
115 *castaneus* (Booker and Keightley 2018). We inferred the distribution of fitness effects (DFE) for
116 deleterious and advantageous mutations occurring in protein-coding genes and gene regulatory
117 elements, by analysing the frequency distribution of derived allele frequencies (the unfolded site
118 frequency spectrum, uSFS). Based on analysis of the uSFS, we found that a model of positive
119 selection was insufficient to explain the troughs in nucleotide diversity around protein-coding
120 exons or conserved non-coding elements (CNEs). However, we found that infrequent, strongly
121 beneficial mutations, which have negligible effect on the uSFS, potentially could do so (Booker and
122 Keightley 2018). This is because infrequent, strongly advantageous mutations may substantially
123 influence diversity at linked sites, while making very little contribution to the uSFS. We concluded
124 that the parameters of positive selection are very difficult to accurately estimate from the uSFS
125 alone (Booker 2020). To understand the relative strengths of selection acting on protein-coding
126 versus gene regulatory regions, the analysis of a model of selective sweeps fitted to patterns of
127 neutral genetic variability may be more powerful.
128
129 In this study, we examine the reductions in nucleotide diversity surrounding protein-coding exons
130 and conserved non-coding elements in wild mice, and attempt to tease apart the modes of
131 selection operating on the two different elements. We fitted a model of selective sweeps to the
132 patterns observed in *M. m. castaneus,* while correcting for the confounding effects of BGS. Our

analysis provides evidence that the strength of selection acting on beneficial mutations in protein-coding exons is far greater than that acting on conserved non-coding elements. Using a simple model of the fitness change brought about by positive selection, we find that selection on protein-coding regions may contribute more to fitness change, despite positive selection occurring more frequently in regulatory regions of the genome. We then compared patterns of putatively neutral diversity among the principal subspecies of *Mus musculus* and their sister species *Mus spretus*. We find that the profiles of nucleotide diversity and the inferred distributions of fitness effects among each group are similar, suggesting that the contributions of positive selection to protein-coding and regulatory change are similar in the different mouse taxa. Note that our goal in this study is not to identify the individual loci that selection has recently acted on; for a recent study identifying the targets of recent selection in wild mice see (Lawal et al. 2021).

Results and Discussion

Profiles of genetic diversity around protein-coding exons and conserved non-coding elements in multiple mouse lineages

If different mouse lineages are subject to similar selection pressures, we might expect that they exhibit similar patterns of diversity across their genomes. We thus compared patterns of genetic diversity in populations of the house mouse *Mus musculus* and the sister species *Mus spretus.* We analysed data previously reported by Halligan et al. (2013) and Harr et al. (2016) for the two mouse species, *M. musculus* and *M. spretus.* For *M. musculus*, we analysed samples from the three sub-species, *M. m. castaneus*, *M. m. domesticus* and *M. m. musculus*. The *M. m. castaneus* individuals (n = 10) were from Himachal Pradesh, India. For *M. m. domesticus,* populations were sampled in France (n = 8), Germany (n = 8) and Iran (n = 8). In the case of *M. m. musculus,* populations were sampled in Afghanistan (n = 6), the Czech Republic (n = 8) and Kazakhstan (n = 8). The *M. spretus* individuals were sampled in Spain (n = 8). We refer to the different sub-populations of *M. m. domesticus* and *M. m. musculus* by the countries where the individuals were sampled.

We identified conserved non-coding elements (CNEs) in murid rodents using a 40-way alignment of placental mammals by means of the *phastCons* approach (Siepel et al. 2005). Following Williamson et al. (2014), the genomes of *M. musculus* and other rodents were masked in the alignment to limit ascertainment bias affecting elements that have recently diverged in the rodent lineage. CNEs identified using *phastCons* overlap with features such as promoters and enhancers (Lindblad-Toh et al. 2011), and thus are likely to have roles in the regulation of gene expression.

For each of the mouse taxa, we examined putatively neutral nucleotide diversity (π) in genomic regions surrounding protein-coding exons and CNEs using the methods described by Halligan et al. (2013). Briefly, polymorphism data were extracted in genomic windows surrounding protein-coding exons and CNEs. We masked any putatively functional sites from analysis windows; these included the exons (including UTRs) of genes annotated in the *M. musculus* genome by ENSEMBL in release 93 (Howe et al. 2021) and CNEs. For each analysis window, we calculated the genetic map distance between the centre of the window and the focal functional element, assuming either the pedigree-based recombination map for *M. musculus* constructed by Cox et al. (2009) or a recombination map estimated using linkage disequilibrium (LD) in the *M. m. castaneus* genome

176 (Appendix). We excluded analysis windows that had a scaled genetic distance of $4N_er < 1$, because
177 downstream analyses assume that sites are not tightly linked. All remaining analysis windows
178 were collated into genetic distance bins. The average number of pairwise differences (i.e.
179 nucleotide diversity) and nucleotide divergence from *Rattus rattus* were calculated for each
180 genetic distance bin. For all analyses, we only examined the autosomes. Downstream analyses
181 were sensitive to the assumption of a single mutation rate, so we excluded hypermutable CpG-
182 prone sites from our analyses, identified as sites that were preceded by a C or succeeded by a G in
183 the 3' to 5' direction in the reference genome (see Materials and Methods).
184
185 The choice of recombination map had a substantial effect on the profiles of average nucleotide
186 diversity observed around protein-coding exons and CNEs (Figures S1, S2). When assuming the
187 pedigree-based Cox map, we found that nucleotide diversity was slightly higher in the immediate
188 flanks of both exons and CNEs (with distances calculated using the estimated recombination
189 frequency), and lower in regions far from functional elements, compared to results with the LD-
190 based map (Figure S1, S2). These differences are consistent with the possibility that the Cox map,
191 which was constructed with a far smaller number of markers than the LD-based map, does not
192 fully capture genomic regions that have either unusually low or high recombination rates. A
193 possible consequence of this would be that analysis windows at intermediate distances from
194 functional elements may appear to be more tightly linked to those elements than they actually
195 are. This is supported by differences in numbers of sites falling into various genetic distance bins
196 between the pedigree-based and LD-based recombination maps (Figures S1 and S2). However,
197 both selective sweeps and BGS can induce LD, and may thus downwardly bias recombination rate
198 estimates obtained using LD-based approaches (Clark et al., 2010). For this reason, we focus on
199 results obtained assuming the pedigree-based Cox map for the remainder of the paper. We
200 present parallel analyses, which assume the LD-based map, in the supplement and describe
201 differences between the respective conclusions in the Discussion.
202
203 All mouse taxa exhibited dips in nucleotide diversity around protein-coding exons and CNEs
204 (Figure 1). To quantify the relative reduction in diversity for each taxa, we calculated π/π_{Ref}, the
205 ratio of π to the average π at distances greater than $4N_er = 1{,}500$ and less than $4N_er = 2{,}500$ for
206 exons, and distances greater than $4N_er = 150$ and less than $4N_er = 250$ for CNEs. The distances for
207 determining π_{Ref} were chosen based on where π began to flatten off with increasing distance from
208 functional elements. Despite the existence of large differences in genome-wide diversity between

209 the taxa, troughs in π/π_{Ref} around exons and CNEs were very similar among mouse lineages
210 (Figures 1, S1, S2). Nucleotide diversity was reduced by 20-30% and 10-20% around protein-coding
211 exons and CNEs, respectively (Figure 1). The dips in diversity extended to genetic distances of up
212 to approximately $4N_er$ = 1,000 around exons, but only to $4N_er$ = 100 around CNEs (Figure 1).
213 Consistent with Halligan et al. (2013), we observed little reduction in between-species divergence
214 around the edges of protein-coding exons, suggesting that mutation rate variation is not a
215 substantial driver of the observed dips in diversity. However, in the immediate flanks of CNEs, we
216 observed a trough in divergence. This may be explained if the *phastCons* approach used to identify
217 CNEs did not readily identify weakly conserved sequences at the edge of more strongly conserved
218 blocks. This would imply that that some sites subject to purifying selection tightly linked to the
219 CNEs may have remained unannotated in our analysis. However, the troughs in nucleotide
220 divergence around CNEs were substantially narrower than the corresponding troughs in diversity.
221 This implies that reduced mutation rates or constrained sites may account for part of the diversity
222 drop around CNEs, but do not explain all of it (Figure S1, S2).
223
224 An important caveat concerning the above analysis is that the mouse taxa thatare subject of the
225 analysis are very closely related, i.e. it has been estimated that the *M. musculus* sub-species
226 complex began to diverge around 350,000 years ago (Geraldes et al, 2011). Furthermore, Geraldes
227 et al (2011) found extensive shared nucleotide variation among the sub-species, and that the
228 average F_{ST} among the members of the sub-species complex ranged from 0.43 to 0.72. Thus,
229 patterns of polymorphism identified in the species are likely to be highly non-independent, and
230 differences in π between the groups presumably reflect fluctuations in population sizes.
231

Figure 1 Nucleotide diversity (π) in regions surrounding protein-coding exons and CNEs in wild mice. Population-scaled recombination rates ($4N_er$) were calculated assuming the recombination map for *M. musculus* constructed by Cox et al. (2009). π_{Ref} is the mean diversity calculated for sites far from functional elements.

Nucleotide polymorphism and divergence in wild mouse genomes

A first step for determining whether there was a consistent signal of natural selection across the mouse genomes, was to identify three classes of functional sites and two classes of putatively neutral sites as follows. For protein-coding gene orthologues between mouse and rat, we identified 0-fold degenerate nonsynonymous sites and UTRs, and used 4-fold degenerate sites as a neutral comparator. Protein-coding sites within the binding motifs of exonic splice enhancers including synonymous sites appear to be subject to purifying selection, implying that 4-fold sites located within them cannot be considered as neutral (Savisaar and Hurst 2018). We therefore excluded all synonymous and non-synonymous sites located within regions that matched such binding motifs. The total numbers of polymorphic and invariant sites that passed filtering for each

250 of the mouse taxa are detailed in Supplementary File 1. We identified sites in the upstream and
251 downstream flanks of individual CNEs for use as neutral comparators (see Methods).
252
253 To determine whether there was a consistent signal of natural selection, we assessed nucleotide
254 diversity and lineage-specific divergence for the three classes of putatively functional sites (Figure
255 2). In all cases, functional site diversity and divergence were lower than for their putatively
256 neutral counterparts, consistent with the action of purifying selection (Figure 2). Note that the *M.*
257 *m. castaneus* data have been analysed in this way before (Halligan et al. 2013; Booker and
258 Keightley 2018) and, as previously reported, *M. m. castaneus* had the highest nucleotide diversity
259 of all *Mus* taxa surveyed (Figure 2; Harr et al. 2016). However, nucleotide divergence reported is
260 the lineage specific divergence accumulated since the focal taxa began to diverge from *Mus*
261 *famulus*, so that divergence estimates for the various mouse taxa are highly non-independent
262 because of shared histories.
263
264 All populations had nonzero Tajima's *D* for putatively neutral sites, indicating the presence of
265 either non-equilibrium population dynamics or genome-wide effects of selection (Figure 2). Mouse
266 populations from Western Europe and Kazakhstan exhibited positive Tajima's *D* for all classes of
267 sites (Figure 2), consistent with a recent history of admixture between different populations or
268 population bottlenecks (Charlesworth and Charlesworth 2010, pp.290-291). A population
269 structure analysis of the mice analysed in this study did not suggest strong admixture between the
270 sampled groups (Harr et al. 2016), but we cannot rule out the possibility of admixture with other
271 unsampled mouse populations. *M. m. castaneus* and populations sampled in Iran and Afghanistan
272 had strongly negative Tajima's *D* values, consistent with recent population expansion or a
273 genome-wide effect of recurrent selective sweeps (Charlesworth and Charlesworth 2010, pp.290,
274 414). Indeed, simulations modelling *D. melanogaster* populations have shown that recurrent,
275 strong selective sweeps can induce negative Tajima's *D* as large as -0.156 at synonymous sites
276 (Campos and Charlesworth 2019). It worth noting that Tajima's *D* is sensitive to the number of
277 individuals and nucleotides analysed (Simonsen et al. 1995), which vary among the mouse taxa, so
278 it is not straightforward to interpret differences in demographic history or strength of selection
279 from these data.
280

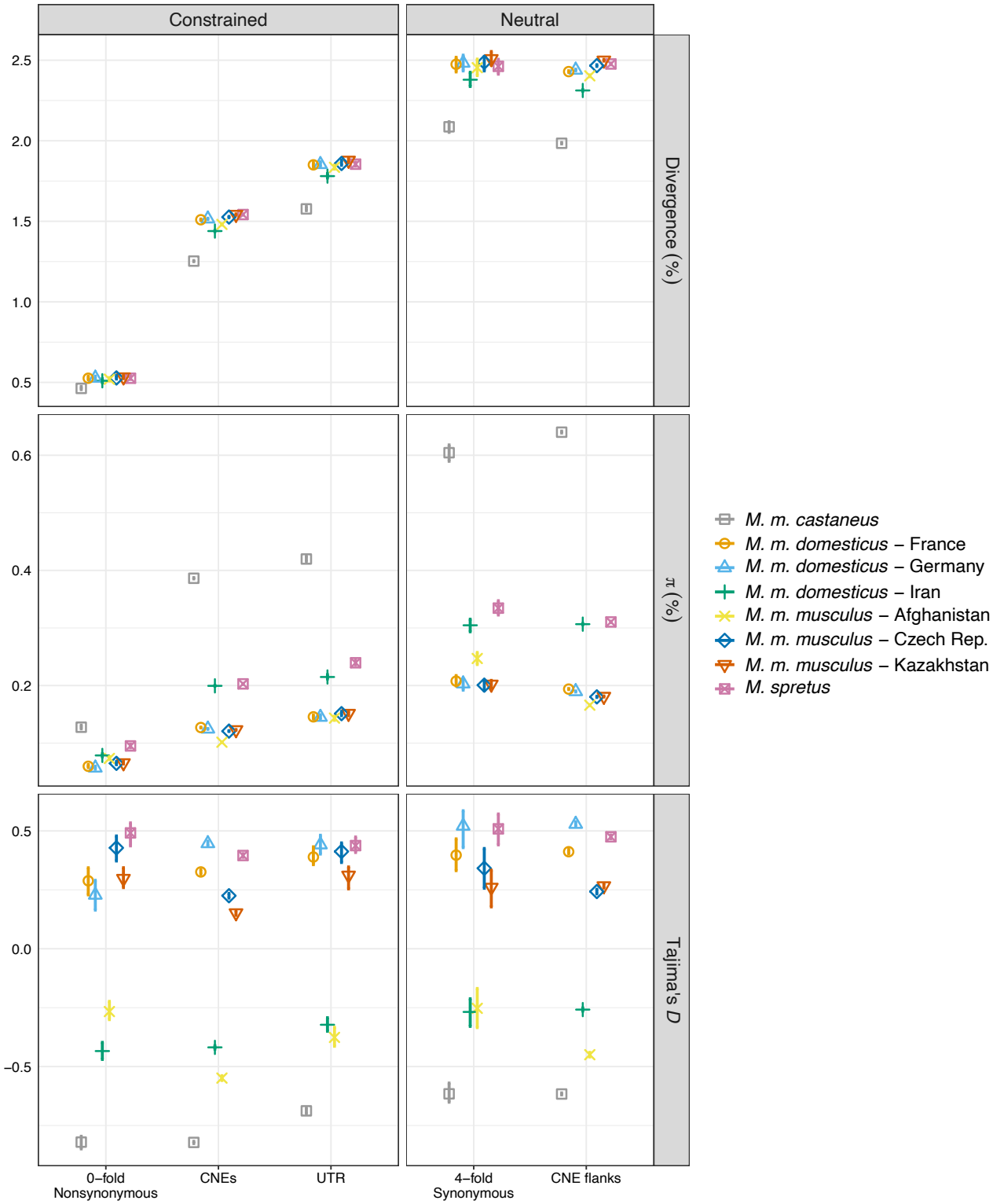

Figure 2 Population genetic summary statistics for three classes of putatively functional sites in the mouse genome and two putatively neutral comparators. Nucleotide diversity (π) and Tajima's *D* are also shown. Error bars represent 95% confidence intervals based on 100 bootstrap samples. Those not visible are shorter than the height of the points.

287 The distribution of fitness effects for deleterious mutations inferred from the uSFS

288 To parameterise a model of BGS, we estimated the distribution of fitness effects (DFE) for
289 deleterious mutations in each of the mouse taxa by fitting a model of mutation-selection-drift
290 balance to the unfolded site frequency spectrum (uSFS). The uSFS is a vector of 0, 1, 2, …, *k* counts
291 of derived alleles, where *k* is the number of haploid genomes sampled. Estimates of the DFE can
292 be obtained by contrasting the uSFS for a selected class of sites and a neutral comparator. Here,
293 we estimated the uSFS for the three classes of functional sites and their putatively neutral
294 comparator sequences. For each class of sites, we fitted a gamma distribution of deleterious
295 mutational effects using *polyDFE* (v2; Tataru and Bataillon 2019). Tataru et al. (2017) showed that
296 *polyDFE* provides robust estimates of the DFE for deleterious mutations based on the uSFS if a
297 discrete class of beneficial mutations is also inferred. While the inferred beneficial mutation
298 parameters are often spurious, including them seems to improve inference of the DFE for
299 deleterious mutations (Booker 2020). Finally, while the gamma distribution is an arbitrary choice
300 of model, and other probability distributions may give better fits to the data, it can capture the
301 important features of the DFE, even if the underlying distribution is multi-modal (Kousathanas and
302 Keightley 2013). Additionally, using the same probability distribution across taxa provides a
303 consistent framework for comparing molecular evolution in the different mouse groups.
304
305 The estimated DFEs were all highly leptokurtic and had similar estimated parameters across the
306 different taxa (Figure 3; Supplementary Table 2). Using *polyDFE,* the DFE is estimated in terms of
307 the scaled selection coefficient for deleterious mutations, $2N_es_d$, where s_d is the reduction in
308 fitness experienced by an individual homozygous for the mutation (which is assumed to be semi-
309 dominant). Figure 3 shows the distribution of effects of deleterious mutational effects discretised
310 into three ranges; nearly neutral mutations with $2N_es_d < 1$, mildly deleterious mutations with $1 \leq$
311 $2N_es_d < 10$ and mutations with $2N_es_d \geq 10$. Consistent with previous studies, amino-acid changing
312 mutations were found to have the highest probability of having strongly deleterious effects
313 (Halligan et al. 2013) and non-coding elements (UTRs and CNEs) had higher fractions of nearly
314 neutral mutations (Figure 3). For 0-fold degenerate sites and CNEs, *M. m. castaneus* had the
315 smallest proportion of nearly neutral variants among the taxa. The DFE inferred for the *M. m.*
316 *musculus* sample from Afghanistan had the highest proportion of strongly deleterious mutations in
317 UTRs, but this may reflect sampling error, since there were only 6 individuals and the population
318 had among the lowest levels of nucleotide diversity (Figure 2).
319

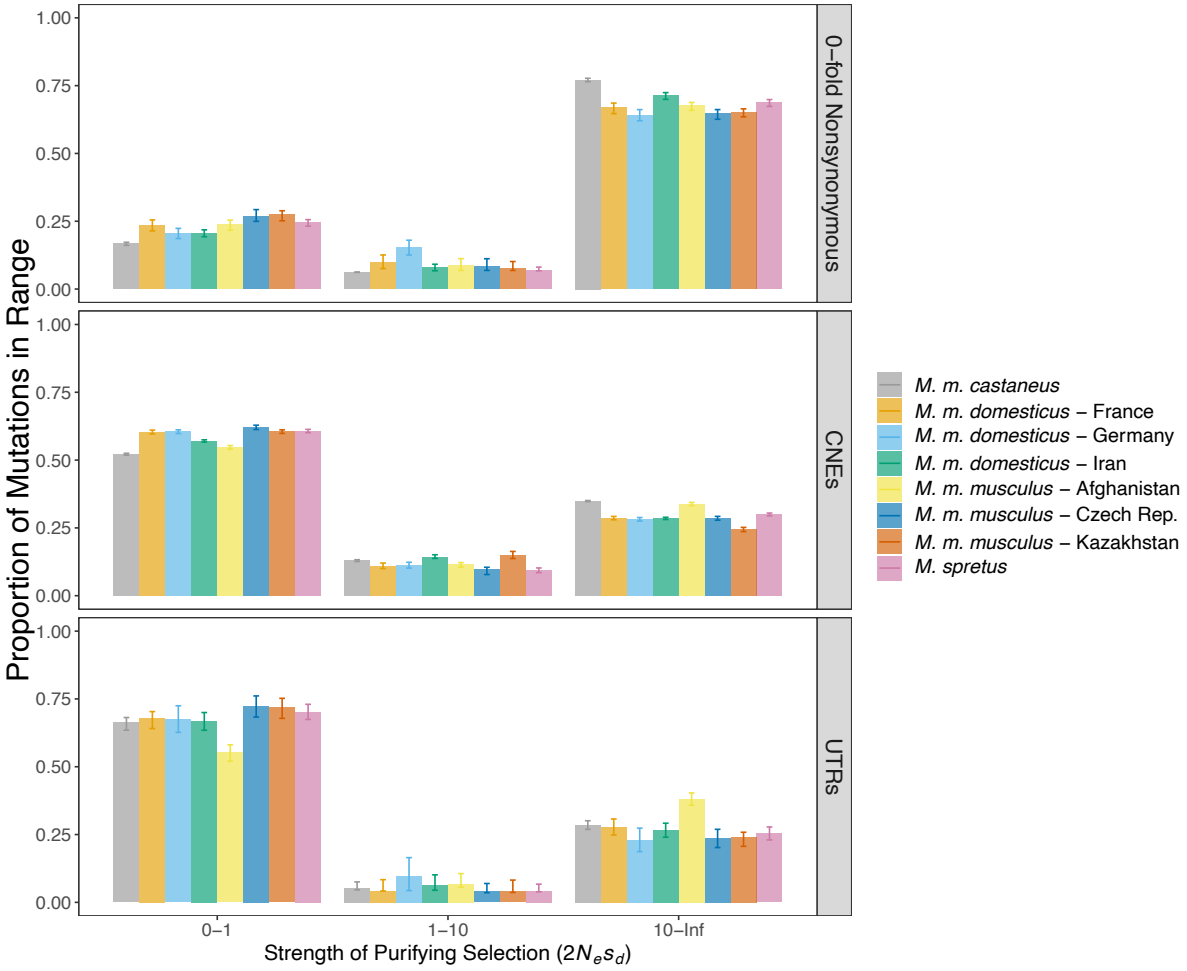

Figure 3 Graphical representation of the distribution of fitness effects of deleterious mutations for three classes of functional sites in wild mice. The figure shows the proportion of mutations falling into three ranges of effect size assuming a gamma DFE for each taxa and class of sites. Error bars indicate the 95% range based on 100 bootstrap replicates.

The contribution of background selection to patterns of diversity around functional elements

Using the inferred DFE parameters for deleterious mutations, we can estimate the contribution of BGS to reductions in nucleotide diversity across the mouse genome. Specifically, we used simulations modelling *M. m. castaneus* to estimate the contribution of BGS to troughs in diversity observed around functional elements (Figure S3). Our simulations incorporated recombination rate variation (assuming either the pedigree-based or LD-based recombination maps, see below), the distribution of exons, UTRs and CNEs in the mouse genome, and the distributions of fitness effects for deleterious mutations estimated for those elements. We estimated values of π around both exons and CNEs from simulated data in the same manner as for the empirical data. Using the

simulation results, we estimated the reduction in diversity caused by background selection, *B,* around functional elements for each genetic distance bin. We calculated $B = \pi/\pi_0$, where π is the nucleotide diversity observed in the simulation and π_0 is the neutral expectation. As we found previously (Booker and Keightley 2018), BGS could not fully explain the reductions in diversity observed around protein-coding exons or CNEs (Figure S3).

Inferences about the strength of BGS made under the assumption of constant population size be misleading if there has been recent population size change. For example, a population bottleneck may lead to the accumulation of weakly deleterious mutations if drift overwhelms selection. As population size increases after a bottleneck, rapid purging of weakly deleterious mutations can occur, leading to deviations from the expectations of standard models of BGS, which assume constant population size (Torres et al. 2020; Johri et al. 2021). We have previously inferred a model of demographic history for *M. m. castaneus*, which suggested that population size has recently increased following a bottleneck (Booker and Keightley 2018). We performed an additional set of simulations incorporating this demographic history, but found that the relative reductions in diversity around both protein-coding exons and CNEs were very similar to those observed under constant population size (Figure S4). Note that the trajectory of the demographic history (bottleneck followed by recovery) we inferred may be an artefact of BGS (Ewing and Jensen 2016; Johri et al. 2021). However, we proceeded with our analysis assuming estimates of *B* for a constant population size, because the variations in *B* around exons and CNEs were very similar with or without population size change.

Parameters of beneficial mutations obtained from patterns of nucleotide diversity

We estimated the parameters of beneficial mutations occurring in protein-coding and gene regulatory regions by fitting a model that combines the effects of BGS and recurrent selective sweeps to troughs in average nucleotide diversity around functional elements (see Materials and Methods). The model quantifies the reduction in neutral diversity surrounding the average exon or CNE, assuming that they are 150bp and 52bp long, respectively. A key parameter in the model is $\pi_0 = 4N_e\mu$, the nucleotide diversity expected under neutrality in the absence of selection at linked sites, where N_e is the effective population size and μ is the mutation rate per basepair. Estimation of π_0 is problematic, however, and π_0 may even be unobservable in empirical data, given the ubiquity of selection at linked sites (Kern and Hahn 2018). In the empirical data, π levelled off at

368 different values for protein-coding exons and CNEs (Figure 1, S1, S2). However, our simulations
369 predicted that *B* should plateau at around 0.95 in genomic regions surrounding both protein-
370 coding exons and CNEs (Figure S3). *B* was not predicted to plateau at 1.0 in our simulations,
371 because we modelled the distribution of all functional elements in the genome, so that a site may
372 be influenced by BGS generated by many surrounding elements. Our simulations did not model
373 sweeps, so simply dividing empirical π by our estimated *B* would give an underestimate of π_0,
374 because the reduction in diversity caused by positive selection was not included. When analysing
375 variation in π, we therefore assumed values of π_0 = 0.0081 and 0.0091 for protein-coding exons
376 and CNEs, respectively, to reflect the different levels at which diversity plateaued.
377
378 We proceeded to fit models combining BGS and selective sweeps to the troughs in diversity
379 around protein-coding exons and CNEs in *M. m. castaneus* assuming various models for the effects
380 of advantageous mutations. We estimated the strength of selection acting on new, semi-dominant
381 beneficial mutations as $\gamma_a = 4N_e s_a$, where s_a is the increase in relative fitness experienced by
382 heterozygotes. We also estimated p_a, the proportion of new advantageous mutations in a
383 functional element. We found that a model with two classes of advantageous mutations gave a
384 better fit than a single class of mutations or an exponential distribution of effects (as judged by
385 AIC; Supplementary File 3). This result held regardless of the recombination map that was
386 assumed (Supplementary File 3).
387

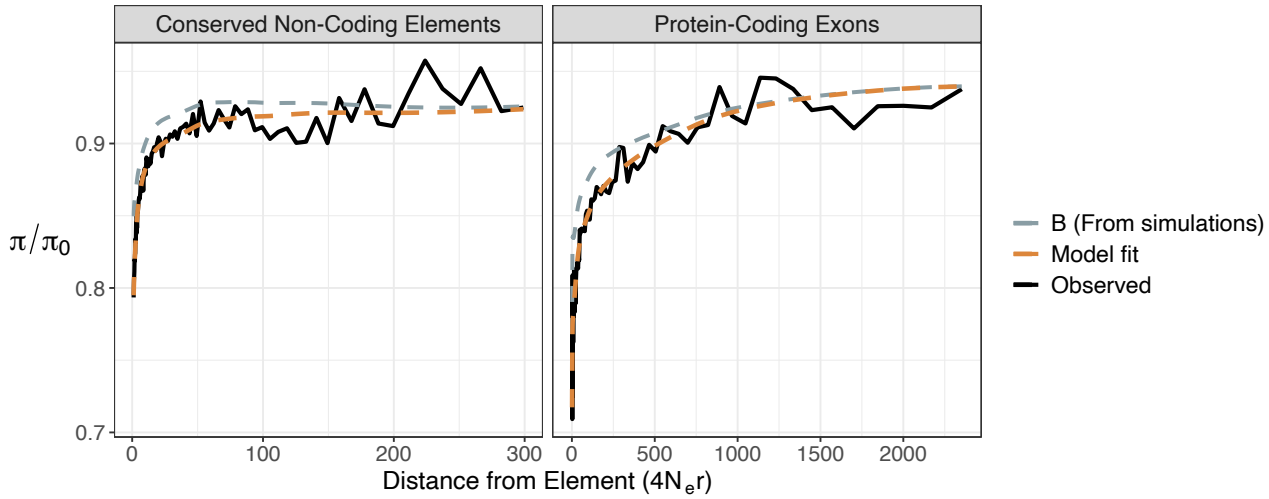

388
389 **Figure 4** The reduction of scaled nucleotide diversity around protein-coding exons and CNEs in *M.*
390 *m. castaneus*, predicted by fitting a model combining the effects of background selection and
391 selective sweeps to the observed data. Genetic distances were calculated assuming the pedigree-

392 based recombination map constructed by Cox et al. (2009). The effect of background selection (*B*)
393 was estimated using simulations.
394
395 For both protein-coding exons and CNEs, we found that the best fitting model included a class of
396 strongly advantageous mutations and a class of more mildly beneficial mutations (Table 1). When
397 assuming the pedigree-based Cox map, we estimated the scaled fitness effects of the strongly
398 selected class (γ_a) to be 6,200 and 1,900 for protein-coding exons and CNEs, respectively. The
399 proportions of mutations with these selection coefficients were 9×10^{-6} and 3×10^{-4}, respectively.
400 The more mildly beneficial class of mutations inferred for protein-coding exons and CNEs had
401 scaled effects of 210 and 7.0, respectively, and the proportion of mutations with these effects
402 were 3.5×10^{-4} and 1.8×10^{-2}, respectively. In the case of CNEs, although two classes of
403 advantageous mutational effects gave the best fit to the data, the coefficient of variation for the
404 parameter estimates of the mildly selected class was large, and evidence for mildly beneficial
405 mutations is fairly weak in this case (Table 1).
406
407 The choice of recombination map strongly affected the estimated selection parameters obtained.
408 Use of the pedigree-based Cox map resulted in estimated selection coefficients that were typically
409 smaller than those obtained when assuming the LD-based recombination map (Supplementary
410 Table 3). This is because we found the troughs in diversity around both exons and CNEs were
411 shallower when calculating genetic distances using the pedigree-based map than when using the
412 LD-based map (Figure S1, S2).
413
414 BGS appears to contribute to the troughs in diversity around both protein-coding exons and CNEs
415 and causes an overall reduction in neutral diversity (Figure 4). Ignoring the contribution of BGS
416 (i.e. by setting *B* to 1.0 when fitting Equation 4 to the diversity troughs) resulted in a much poorer
417 model fit (Supplementary File 3). In the absence of BGS, the selection coefficients for
418 advantageous mutations required to explain the observed data are, as expected, far higher
419 (Supplementary File 3).
420
421
422
423

424 **Table 1** Parameters of positive selection in *M. m. castaneus* estimated by fitting a model of
425 selective sweeps and background selection to troughs in diversity around functional elements. The
426 frequency (p_a) and scaled selection coefficients (γ_a) for the two classes of advantageous effects are
427 given. Standard errors are shown in square brackets below point estimates.
428
429

Element	$\gamma_{a,1}$	$p_{a,1}$	$\gamma_{a,2}$	$p_{a,2}$
Protein-Coding Exons	6,170	0.80×10^{-5}	208	3.50×10^{-4}
	[2,650]	[0.50×10^{-5}]	[105]	[1.80×10^{-4}]
CNEs	1,910	1.30×10^{-5}	7.00	1.78×10^{-2}
	[673]	[0.60×10^{-5}]	[3.50]	[1.29×10^{-2}]

430
431 We did not include gene conversion events in our analysis, because gene conversion tracts, which
432 have an estimated mean length in mice of 135bp (Paigen et al. 2008), are relatively short
433 compared to the genetic distances we analysed (up to 100,000bp and 5,000bp for exons and CNEs,
434 respectively). Furthermore, the ratio of the rates of gene conversion and crossover events has
435 been estimated to be 0.105 in mice (Paigen et al. 2008). Overall, gene conversion is expected to
436 contribute little to the net frequency of recombination between neutral and selected sites.
437
438 The relative contribution of adaptive substitutions in protein-coding and regulatory regions
439 to fitness change in mice

440 An important goal of evolutionary biology is to understand the extent to which protein-coding and
441 regulatory elements contribute to phenotypic evolution (King and Wilson 1975; Wray 2007; Stern
442 and Orgogozo 2008; but see Hoekstra and Coyne 2007). Using our estimated selection parameters,
443 we can parameterise the following model of the rate of fitness change per generation (ΔW)
444 brought about by the fixation of advantageous mutations. For a particular class of sites, assume
445 there are η_a nucleotides in the genome at which new mutations occur at rate μ per nucleotide site
446 per generation. If the size of the breeding population is N, then $2N\mu$ new mutations enter the
447 population each generation. We assume that a proportion of the new mutations, p_a, is strongly
448 advantageous, with a selection coefficient of s_a in heterozygous carriers. When the effectiveness
449 of selection exceeds that of genetic drift ($2N_e s_a > 1$), the fixation probability is approximately $2s_a$
450 (Haldane 1927). Once fixed, advantageous mutations increase population mean fitness by s_a / h,
451 where h is the dominance coefficient, giving the following expression:

452

453 $$\Delta W = \frac{4N\mu p_a \eta_a s_a^2}{h} \quad (1).$$

454

455 Since we are interested in the relative contribution to fitness change, and assumed that the
456 average point mutation rate is the same for CNEs and protein-coding exons, we can thus ignore μ
457 in Equation 1. Note that the above model is conceptually similar to an approach taken by Lynch et
458 al. (1993) to model fitness change under mutational meltdown. We parametrized Equation 1 using
459 our estimated selection parameters. Note that we estimated two classes of beneficial mutational
460 effects for the two classes of functional elements. When parameterizing Equation 1, we summed
461 the fitness contributions over the two classes of fitness effect inferred for each element. We
462 calculated the ratio of ΔW for protein-coding exons and CNEs ($\Delta W_{Exons}/\Delta W_{CNEs}$) as a measure of
463 the relative contributions of the two types of elements to adaptive evolution (which also implicitly
464 assumes the same h for all classes of mutation).

465

466 Our point estimates suggest that ΔW is larger for protein-coding regions than regulatory regions.
467 However, it is notable that the total genomic rate of fixation of beneficial mutations is higher for
468 CNEs than for coding regions (see also Halligan et al. 2013), but this reflects the fact that there are
469 approximately three times as many CNE bases as non-synonymous bases in the mouse genome.
470 Although the estimated genomic rate of fixation of beneficial mutations in CNEs is greater than
471 that of protein-coding exons (Table 2), the average strength of selection acting on a new
472 advantageous nonsynonymous mutation far exceeds that of CNEs (Table 2). Fitness change is
473 proportional to the square of the effect size, so that the change in population mean fitness
474 brought about by the fixation of advantageous mutations is substantially higher for protein-coding
475 exons than for CNEs. This result is sensitive to the choice of recombination map, since we inferred
476 stronger selection when assuming the LD-based map (Supplementary Table 3). Using a parametric
477 bootstrap approach, we found that $\Delta W_{Exons}/\Delta W_{CNEs}$ was significantly greater than 1 when using
478 the LD-based map, but not when assuming the pedigree-based map of Cox et al. (2009).

479

480 **Table 2** Estimates of the change in fitness brought about by the fixation of advantageous
481 mutations. Estimates were obtained assuming an effective populations size for *M. m. castaneus* of
482 420,000 and the selection parameters shown in Table 1.

483

Recombination Map	Element	$\Delta W_{Exons}/\Delta W_{CNEs}$	95% Bootstrap interval
LD-based (*castaneus* map)	Protein-Coding Exons / CNEs	23.11	11.08 - 54.67
Pedigree-based (Cox et al. 2009)	Protein-Coding Exons / CNEs	2.94	0.211 - 46.36

484

485

486 Selective sweeps and background selection in the mouse genome

487 The profiles of nucleotide diversity indicate the existence of pervasive effects of selection on
488 diversity across the genome (Figure 1, Figure 2). By fitting a model of sweeps to the troughs in
489 diversity around protein-coding exons and CNEs, while assuming that the troughs are partly
490 caused by BGS, we estimated the parameters of positively selected mutations occurring in the two
491 classes of element. Our analysis suggests that regulatory sequences experience a higher genomic
492 rate of newly arising advantageous mutations than protein-coding sites. However, the trough in
493 diversity around exons is both deeper and wider than what is observed around CNEs, and,
494 accordingly, we found that protein-coding regions experience more strongly selected mutations
495 than regulatory sequences. Using a different approach, Campos et al. (2017) came to a similar
496 conclusion for *D. melanogaster* by comparing UTRs with the coding sequences of genes.

497

498 Due to non-independence among the various *M. musculus* sub-species, we only estimated
499 parameters of positive selection for *M. m. castaneus,* the sub-species with the highest levels of
500 diversity. Our selection parameter estimates for *M. m. castaneus* are fairly similar to estimates
501 obtained for European *M. m. domesticus* in an earlier study (Teschke et al. 2008).

502

503

504 ## Limitations and next steps

505 There are a number of caveats concerning our estimates of positive selection parameters. Firstly,
506 we found that an exponential distribution of beneficial mutational effects provided a poorer fit to
507 the troughs in diversity compared to a model with two discrete classes of effects (Supplementary
508 File 3). However, the true DFE for advantageous mutations is almost certainly more complex than
509 the simple models assumed. The approach used in this study was based on average nucleotide
510 diversity across many sites, and we presumably had little power to infer a more complex model of
511 the DFE for advantageous mutations. Secondly, we have assumed that all elements of a particular
512 class share a common set of selection parameters. This is problematic, since CNEs could be
513 composed of several categories, such as promoters and enhancers, which may be subject to
514 different selective pressures. Indeed, different categories of protein-coding genes may also be
515 subject to different selection pressures. For example, immunity genes in *D. melanogaster*, virus
516 interacting proteins in humans and highly expressed genes in *Capsella grandiflora* appear to have
517 higher rates of adaptive substitutions than the respective genome wide averages (Enard et al.
518 2014; Obbard et al. 2009; Williamson et al. 2014). Thirdly, for a single class of advantageous
519 mutational effects, under the assumption that there is no interference among sweeps, the
520 predicted reductions in diversity caused by selective sweeps can be modelled as a simple
521 hyperbolic function (Equation 4). However, if the rate of sweeps is sufficiently high, and the rate of
522 recombination is sufficiently low, selective interference can cause the rate of sweeps to be lower
523 than predicted by a given strength of selection (Campos and Charlesworth 2019). This implies that
524 the strength of positive selection would be overestimated by our methods. A bias in the opposite
525 direction, which is likely to be more important for genomic regions with normal levels of
526 recombination, is caused by deviations from one of the assumptions underlying Equation 4, i.e.
527 that there is full recovery of nucleotide diversity between selective sweeps (Campos and
528 Charlesworth 2019; Charlesworth 2020). This would lead to the effects of sweeps to be
529 underpredicted. Incorporating more sophisticated models of selective sweeps into the inference
530 framework is a logical next step.

531

532 The architecture of functional elements in the mammalian genome is such that a single exon or
533 CNE is rarely far away from another functional element. When estimating the effects of sweeps on
534 neutral diversity, we excluded all putatively functional sites from our analysis windows, but
535 multiple linked elements may affect observed diversity at a given locus. For this reason, we did not

536 estimate the strength of positive selection acting on UTRs, although sweeps in these elements are
537 also likely to contribute to heterogeneity in π across the mouse genome, as has been found in *D.*
538 *melanogaster* (Campos et al. 2017). The model fitted to the troughs in diversity assumes that
539 selection is generated by a single, idealised exon or CNE. However, there is variation in the length
540 of exons and CNEs across the genome. An analysis that models genome-wide heterogeneity in
541 diversity while taking into account the locations of individual functional elements, similar to the
542 method developed by Elyashiv et al. (2016) for *D. melanogaster*, could be a more powerful
543 approach. Note that the approach of Elyashiv et al. (2016) might not be applicable in all situations,
544 because it conditions the effects of sweeps on the locations of recent substitutions. In mice and
545 humans, patterns of diversity around nonsynonymous substitutions are indistinguishable from the
546 patterns of diversity around synonymous substitutions (Hernandez et al. 2011; Halligan et al.
547 2013). Developing a chromosome-wide analysis that conditions the effects of sweeps on the
548 locations of genomic elements rather than substitutions may be a useful avenue for further
549 research.
550
551 The model of sweeps we assumed involves positive selection acting on *de novo* mutations – the
552 so-called `hard', or `classic' sweep model. Studies in humans and *Drosophila* have, however,
553 suggested that 'soft' sweeps are common (Garud et al. 2015; Garud and Petrov 2016; Schrider and
554 Kern 2016; but see Harris et al. 2018). Soft selective sweeps occur when advantageous alleles
555 present in multiple copies in the population spread to fixation, which can occur if selection acts on
556 standing genetic variation or if multiple copies of the selected allele arise independently
557 (Hermisson and Pennings 2017). Additionally, adaptation acting on quantitative traits subject to
558 stabilising selection may generate partial sweeps, because changes in allele frequencies at many
559 loci can rapidly alter mean phenotypes, without necessarily causing fixations (Pritchard et al. 2010;
560 Jain and Stephan 2017) . The profiles of the reductions in diversity around soft and partial sweeps
561 differ from those expected under hard sweeps, and if either of the alternative types of sweep
562 were common, the assumption of a hard sweep model could result in spurious parameter
563 estimates (Elyashiv et al. 2016). Finally, the trough in diversity around a selective sweep in a
564 structured population is expected to be shallower than in a panmictic population because of the
565 longer time taken to reach fixation (Barton 2000; Santiago and Caballero 2005). If beneficial alleles
566 are frequently introduced via migration, we may therefore underestimate the strength of
567 selection.
568

569 Finally, it is important to note that CNEs are generally expected to represent regulatory sequences
570 that are deeply conserved. It has been demonstrated that the evolution of regulatory elements is
571 more dynamic than that of coding sequences, with major gains of new regulatory elements having
572 occurred in vertebrate and mammalian evolution (Mikkelsen et al. 2007; Lowe et al. 2011). If more
573 recently acquired regulatory elements, which may be absent from the CNE dataset, experience
574 stronger or more frequent adaptive substitutions, it is possible that we have underestimated the
575 contribution of regulatory changes to adaptive evolution. For instance, a recent gain of a new
576 regulatory element might have been caused by relatively strong positive selection acting on the
577 element as a whole, resulting in a single sweep event. This would fall outside the inference
578 framework developed here.
579
580 It seems likely that adaptation does not fit any one particular mode, but rather different functional
581 elements will be subject to a mixture of different types of sweep that may vary depending on the
582 genomic region. For example, adaptation may more commonly act on standing variation in
583 regulatory regions simply because they harbour greater nucleotide diversity than nonsynonymous
584 sites (Figure 2).
585

Conclusions

In this study, we have shown that multiple wild mouse taxa exhibit patterns of genetic diversity and divergence that are consistent with the action of natural selection. Furthermore, we have shown that strong positive selection can explain the dips in diversity around protein-coding exons and CNEs in *M. m. castaneus.* Finally, even though the framework we have adopted here is incapable of distinguishing different modes of positive selection such as adaptation, sexual selection and various forms of competition, the estimated parameters of positive selection suggest that mutations in protein-coding regions may contribute more to the rate of change in fitness under positive selection than regulatory mutations.

Materials and Methods

Genomic data

We re-analysed previously published genome sequences for the 54 wild-caught *Mus musculus* individuals described in Harr et al. (2016) and the 10 *M. m. castaneus* individuals and the *M. famulus* individual originally described in Halligan et al. (2010, 2013). The mouse samples belonged to three species: *Mus spretus, Mus musculus* and *Mus famulus*. The *M. spretus* individuals (*n* = 8) were from Madrid, Spain. The *M. musculus* individuals are composed of samples from the sub-species *M. m. domesticus, M. m. musculus* and *M. m. castaneus*. Three populations of *M. m. domesticus* were sampled (Massif Central, France, *n* = 8; Cologne-Bonn, Germany, *n* = 8; Ahvaz, Iran, *n* = 8) and three populations of *M. m. musculus* were sampled (Afghanistan, *n* = 6; Studenec, Czech Republic, *n* = 8; Mazar-e-Sharif, Kazakhstan, *n* = 8). We also analysed 10 *M. m. castaneus* described by Halligan et al. (2010, 2013), sampled in Himachal Pradesh, India. The one *M. famulus* individual, originated in Southern India, though Halligan et al. (2013) obtained it from the Montpellier Wild Mice Repository.

Harr et al. (2016) published and made available the variant calls obtained from the *M. musculus* samples described above in the form of VCF files. However, Harr et al. (2016) did not include invariant sites in their VCFs; for our purposes we required this information, so we re-called variants from their processed BAM files, available at http://wwwuser.gwdg.de/~evolbio/evolgen/wildmouse/. The data had been processed according to the GATK version 3 best practices pipeline, up to the step prior to variant calling. Briefly, all sequencing reads had been mapped to the *mm10* genome using *bwa-mem* (Li 2013). Reads were then sorted, merged and PCR duplicates were marked using *picardtools* (https://broadinstitute.github.io/picard/). Base Quality Score Recalibration was then applied using the dbSNP resource for mice (https://www.ncbi.nlm.nih.gov/snp) to produce analysis-ready alignments in BAM format. We generated BAM files for the *M. m castaneus* data and the *M. famulus* mice using the same procedure using FASTQ files downloaded from the European Nucleotide Archive (accession number PRJEB2176). For each of the mice, we called variants separately using the HaplotypeCaller tool from GATK3.7 (McKenna et al. 2010), with the options "*– emitRefConfidence BP_RESOLUTION –max-alternate-alleles* 2", and made population-specific

627 VCF files using the GATK tools *combineGVCFs* and *genotypeGVCFs*. We restricted all analyses to
628 autosomal sites.
629
630 ### Outgroup information and CpG sites

631 In this study we used *M. famulus*, *Mus pahari* and *Rattus norvegicus* as the outgroup species. For
632 each of the mouse taxa described above and each outgroup, we created a synthetic mm10-length
633 reference genome by replacing mm10 alleles with the major allele of the variant call set. In
634 addition, we constructed a synthetic genome for *R. norvegicus* by replacing mm10 alleles with the
635 homologous positions in the rat genome using the UCSC reciprocal best alignments between rn6
636 and mm10 (available at:
637 ftp://hgdownload.cse.ucsc.edu/goldenPath/rn6/vsMm10/reciprocalBest/) using custom Python
638 scripts. For an additional outgroup, more closely related to *Mus musculus* than the rat, we
639 obtained the homologous alleles from *Mus pahari* at mm10 positions using the ENSEMBL pairwise
640 alignments between the *M. pahari* reference sequence (Thybert et al. 2018) and mm10 (available
641 at: ftp://ftp.ensembl.org/pub/release-90/maf/ensembl-compara/pairwise_alignments/).
642
643 CpG sites have higher rates of spontaneous mutation than non-CpG sites, and identifying and
644 excluding CpG-prone sites is a conservative way of reducing the impact of CpG hypermutability on
645 analysis of population genomic data (Gaffney and Keightley 2008). For each of the rodent taxa, we
646 used the synthetic mm10-length reference genomes to identify the locations of CpG-prone sites,
647 defined as those sites in our synthetic references that were preceded by a C or followed by a G in
648 the 5' or 3' direction, respectively. All analyses presented in this paper excluded CpG-prone sites.
649
650 ### Annotations and identifying conserved non-coding elements

651 We downloaded the list of mouse-rat orthologs from https://www.ensembl.org/biomart/ and
652 extracted the annotations for each from version 38.93 of ENSEMBL
653 (Mus_musculus.GRCm38.93.gtf.gz; Howe et al. 2021). For each of the orthologs, we identified the
654 positions of 0-fold degenerate nonsynonymous and 4-fold degenerate synonymous sites using the
655 synthetic genomes for each of the mouse taxa and the outgroups described above. The locations
656 of 5' and 3' untranslated regions (UTRs) were retained for downstream analyses. We also retained
657 a list of all exonic positions in the mouse genome, regardless of orthology, for the purposes of
658 filtering out functionally constrained sites in downstream analyses.

659

660 There is evidence that synonymous sites within exonic splice enhancers (ESEs) in humans are
661 subject to purifying selection, and that ignoring ESEs can bias analyses that rely on the assumption
662 that synonymous sites evolve neutrally (Savisaar and Hurst 2018). Savisaar and Hurst (2018)
663 identified putative ESEs by comparing human gene sequences against various lists of ESE motifs.
664 They found that synonymous sites in regions matching ESE motifs had lower nucleotide diversity
665 than those outside of putative ESEs. We identified the locations of potential ESEs in protein-coding
666 genes orthologous between mice and rat using the merged list of ESEs described in Savisaar and
667 Hurst (2018) (kindly provided by Rosina Savisaar). For each of the mouse-rat orthologs, we
668 extracted the gene sequence and performed a string search against the list of ESE motifs. We
669 recorded the genomic position of each region matching an ESE motif and used them to filter out
670 the affected coding sites in downstream analysis.

671

672 We identified conserved non-coding elements (CNEs) in murid rodents using a 40-way alignment
673 of placental mammals downloaded from UCSC
674 (http://hgdownload.cse.ucsc.edu/goldenPath/mm10/multiz60way/). To avoid ascertainment bias,
675 the mouse and rat genomes in the 40-way alignment were converted to the character "N" prior to
676 calling conserved elements, following Williamson et al. (2014). We ran *phastCons* with the
677 following arguments --expected-length=45 --target-coverage=0.3 --rho=0.31. To identify CNEs, we
678 masked all exonic regions from the resulting file of *phastCons* elements using the complete list of
679 annotations from the 38.93 database (see above). The scripts and full pipeline used to identify
680 CNEs are available at https://github.com/rorycraig337/mouse_mm10_conserved_elements.

681

682 For each CNE identified in this way, we obtained the location of their flanking sequences, which
683 we used as neutral comparators in downstream analysis. For each CNE, we recorded the locations
684 of two loci of equal length upstream and downstream of the focal element, offset by 500bp. We
685 merged overlapping CNE-flanks and masked out sites that overlapped any CNE or exonic sites.

686

687 We analysed the mouse genomes assuming the pedigree-based genetic map of *Mus musculus*
688 constructed by Cox et al. (2009). The Cox map was constructed using data from 3,546 meioses
689 observed in crosses of common laboratory strains. The markers genotyped by Cox et al. (2009)
690 were mapped to the mm9 reference genome, but in the present study we converted the mm9
691 coordinates to mm10 positions as follows. The Cox map was downloaded from the Jackson

692 Laboratory website (http://cgd.jax.org/mousemapconverter/). The SNP positions of the Cox map
693 were then extracted and converted to mm10 positions using the online UCSC LiftOver tool
694 (https://genome.ucsc.edu/cgi-bin/hgLiftOver). The physical distances between the mm10 SNP
695 positions were then converted to units of genetic distance using the Jackson Laboratory's
696 conversion tool (http://cgd.jax.org/mousemapconverter/). We also analysed the mouse genomes
697 using an LD-based recombination map inferred from the sample of *M. m. castaneus* individuals, as
698 described in the Appendix.
699

700 ### Mouse analysis – Patterns of nucleotide diversity around selected sites

701 For each of the *M. musculus* sub-species and *Mus spretus*, we examined patterns of nucleotide
702 diversity around protein-coding exons and CNEs. From the edges of protein-coding exons (CNEs),
703 polymorphism data and divergence from the rn6 rat reference genome were extracted in windows
704 of 1Kbp (100bp) extending to distances of 100Kbp (5Kbp). Analysis windows only extended to the
705 midway point between adjacent elements. Sites within the exons of protein-coding genes or CNEs
706 were excluded from analysis windows. The genetic distance between an analysis window and a
707 focal element was calculated either from the pedigree-based genetic map constructed using
708 common lab strains of *M. musculus* (Cox et al. 2009) or the linkage disequilibrium (LD) based
709 recombination map for *M. m. castaneus*. The SFS and divergence from were recorded for each
710 analysis window. Analysis windows were then binned based on the genetic distance from the focal
711 element, and the SFS and divergence from individual windows were collated. Because LD-based
712 and pedigree-based recombination maps have different features and shortcomings (see Results),
713 we performed analyses based on both genetic maps.
714

715 ### Estimating the unfolded site frequency spectrum, summary statistics and the
716 distribution of fitness effects

717 We analysed genetic variation for five different classes of sites in the genome, i.e. the 0-fold and 4-
718 fold degenerate sites and UTRs of protein-coding genes, CNEs and CNE-flanks. For each class of
719 sites, we inferred the unfolded site frequency spectrum (uSFS), which is the distribution of derived
720 allele frequencies in the mouse samples. The uSFS was inferred by maximum likelihood using the
721 two-outgroup method of Keightley and Jackson (2018) using *Mus famulus* and *Mus pahari* as
722 outgroups. We compared the fit of 1-, 2- and 6- parameter mutation rate models using *est-sfs*
723 (v2.03; Keightley and Jackson 2018). Consistently, a model with 6 mutation rate parameters (i.e.

724 the R6 model from Keightley and Jackson 2018) provided the best fit to the data (as judged by
725 model likelihoods), but the uSFS and lineage specific divergences that were estimated under the 2-
726 parameter and 6-parameter models were almost identical in all cases (Supplementary File 1), so
727 we have used the results from the 2-parameter model in our analyses for all taxa. For each taxon
728 and class of sites, we performed 100 bootstraps, sampling genes or CNEs with replacement. We
729 inferred the uSFS for each bootstrapped dataset as above. For each class of sites, we calculated
730 nucleotide diversity (π) and Tajima's *D* from the inferred uSFS for each bootstrap sample.
731
732 Estimates of the distribution of fitness effects (DFE) were obtained by analysing the unfolded site
733 frequency spectrum for each class of functional site using *polyDFE* v2 (Tataru and Bataillon 2019).
734 For 0-fold sites and UTRs, we used 4-fold degenerate synonymous sites as the neutral comparator,
735 and for CNEs we used CNE-flanks. Using *polyDFE2*, we fitted a gamma distribution of deleterious
736 mutations effects and a single class of beneficial mutations (using the -model B option). We
737 excluded between species divergence from the analysis using the "-w" option. We fitted the uSFS
738 data for each of the bootstrap replicates described above.
739
740 Simulating background selection

741 There is substantial evidence that background selection (BGS) contributes to troughs in diversity
742 around protein-coding exons and CNEs (Halligan et al. 2013; Booker and Keightley 2018). For our
743 analysis, we therefore required estimates of the effect of BGS on neutral diversity, *B*, at varying
744 distances from functional elements. Estimates of *B* were included as covariates when fitting a
745 model of selection at linked sites. However, when purifying selection is weak ($\gamma_d < 5$) analytical
746 formulae for calculating *B* over-predict the effects of BGS (Gordo et al. 2002; Good et al. 2014),
747 and weakly deleterious mutations appear to comprise a large fraction of the DFEs for mice (Figure
748 3 and Halligan et al. 2013). We therefore opted to obtain estimates of the variation in *B* from
749 forward-in-time simulations that modelled the entire range of fitness effects inferred for mice.
750
751 We used *SLiM* v3.2 (Haller and Messer 2019) for this purpose. Following Booker and Keightley
752 (2018), we incorporated the actual distribution of functional elements (the coding exons and UTRs
753 of protein-coding genes, and CNEs) and the estimated recombination rates. 1 Mbp regions of the
754 mouse genome were randomly sampled and the functional annotations in the sampled regions
755 were used as the basis of a simulation replicate. The parameters of the gamma distributions of
756 fitness effects for deleterious mutations estimated for 0-fold sites, UTRs and CNEs were used in

757 the simulations for the respective elements. The recombination rate variation present in the
758 sampled region of the mouse genome was included in the simulations using either the pedigree-
759 based map from Cox et al. (2009) or the LD-based recombination map for *M. m. castaneus*. When
760 assuming the Cox map, the recombination rates (in units of cM/Mbp) were scaled in the
761 simulations by a factor of 420r, assuming N_e = 420,000 for wild *M. m. castaneus*. In the case of the
762 LD-based estimates of the recombination rate, population-scaled recombination rates (in units of
763 $4N_er$) were simply divided by 4N, where N was the simulated population size. Populations of N =
764 1,000 diploid individuals were simulated for 20,000 generations. We set the mutation rate such
765 that the neutral expectation $\pi_0 = 4N_e\mu = 0.01$, based on the upper estimate of nucleotide diversity
766 observed in the *M. m. castaneus* genome (Figure 1). Given the simulated population size of 1,000
767 diploids, $4N_e\mu = 0.01$ corresponded to a point mutation rate of $\mu = 2.5 \times 10^{-6}$. We used the tree-
768 sequence recording option in *SLiM* to record the genealogies of the simulated populations, so
769 modelling neutral mutations in *SLiM* was not required. Instead, neutral mutations were added to
770 the recorded coalescent trees at a rate μ using *PySLiM*
771 (https://pyslim.readthedocs.io/en/latest/introduction.html). We sampled 200 haploid
772 chromosomes from the population and extracted $B = \pi/\pi_0$ as a function of genetic distance from
773 both protein-coding exons and CNEs. Data were extracted from the simulated populations in the
774 same way as for the empirical data. To obtain smoothed B values, we fitted LOESS curves to the
775 average π observed around functional elements in the simulated data. We fitted LOESS curves
776 using a span parameter of 0.3 and the number of sites contributing to each analysis bin as weights
777 in R (v3.4.2).
778

779 ### Model of recurrent selective sweeps and background selection

780 Our analysis is a modification of that of Elyashiv et al. (2016) and Campos et al. (2017), where
781 expressions were described for the neutral diversity expected under the combined effects of BGS
782 and sweeps. Consider a haplotype with a set of neutral sites linked to a site that is the target of
783 positive selection. A new, semi-dominant advantageous mutation with heterozygous selection
784 coefficient s_a occurs at site i on the haplotype and spreads to fixation. Recombination between
785 sites i and k uncouples the neutral and selected sites at rate $r_{i,k}$ per generation. The expected
786 change in neutral diversity at site k ($\Delta\pi_k$), relative to its expectation in the absence of selection (π_0)
787 is given by

788 $$\frac{\Delta\pi_k}{\pi_0} = -(4N_e s_a)^{\frac{-2r_{i,k}}{s_a}}. \quad (2)$$

See Barton (2000), Charlesworth and Charlesworth (2010, p411) or Campos and Charlesworth (2019) for derivations of Equation 2. This approximation assumes that selection pressure on the advantageous allele satisfies $N_e s_a >> 1$, so that the sweep can be treated deterministically following an initial stochastic establishment phase. Under this assumption, the quantity $-\Delta\pi_k$ in Equation 1 can be equated to the probability of a sweep-induced coalescent event at site k (Wiehe and Stephan 1993). For a particular class of functional elements (e.g. protein-coding exons), sweeps occur at a rate of $V_a = 2\mu p_a \gamma_a$ per nucleotide per generation (Kimura and Ohta 1971), where μ is the mutation rate per nucleotide site, p_a is the proportion of new mutations that are advantageous and γ_a is the scaled selection coefficient ($4N_e s_a$) for these mutations. If V_a is sufficiently low, such that sweeps do not interfere with each other, the total probability of sweep-induced coalescence for a neutral site caused by selection at a linked functional element is:

$$P_{sc,k} = V_a \tau \gamma_a^{\frac{-2r_{i,k}}{s_a}}, \quad (3)$$

where τ is the number of sites in a particular class of functional element. In our analysis of data from wild mice, $r_{i,k}$ was measured from the end of a functional element to the centre of an analysis window.

The effects of background selection at site k can be represented by multiplying the effective population size by a factor B_k. The probability of coalescence for a neutral allele affected by BGS is thus $1/(2B_k N_e)$. We assume that coalescent events caused by BGS and sweeps follow independent exponential distributions, so thar the rate of coalescence induced by the two processes is the sum of $1/(2B_k N_e)$ and $P_{sc,k}$. We also multiply the sweep effect $P_{sc,k}$ by B_k to reflect the reduction in the fixation probability of a new advantageous mutation as a result of the reduction in N_e caused by BGS, following Kim and Stephan (2000). Simulations show that this may overestimate the effect of BGS on fixation probabilities (Campos and Charlesworth 2019), we thus compared selection parameters with and without including background selection.

Writing the reciprocal of the rate of coalescence at the neutral site under the combined effects of BGS and sweeps as T_k (which is equivalent to the expected time to coalescence of a pair of alleles), and expressing it relative to the expected time to coalescence under neutrality (T_0), we have:

$$\frac{T_k}{T_0} \approx \frac{\pi_k}{\pi_0} \approx \frac{1}{B_k^{-1}+2N_e B_k P_{sc,k}}. \quad (4)$$

We estimated parameters of advantageous mutations by fitting Equation 4 to the relationship between nucleotide diversity and genetic distance from functional elements, using non-linear least squares with the *lmfit* (v0.9.7) package for Python 2.7. When modelling a single class of fitness effects, we estimated γ_a and p_a using Equation 4. To incorporate two discrete classes of advantageous mutational effects, we modified Equation 4, replacing $P_{sc,k}$ in Equation 4 with

$$P_{sc,k} = V_{a,2}\tau\gamma_{a,2}^{\frac{-2r_{i,k}}{s_{a,2}}} + V_{a,2}\tau\gamma_{a,2}^{\frac{-2r_{i,k}}{s_{a,2}}}, \quad (5)$$

where the subscripts 1 and 2 refer to the two different classes of fitness effects.

To model an exponential distribution of fitness effects, we replaced $P_{sc,k}$ with

$$P_{sc,k} = \int_0^\infty V_a\tau\gamma_a^{\frac{-2r_{i,k}}{s_a}} \phi(\gamma_a|\,\bar{\gamma}_a)\mathrm{d}\gamma_a, \quad (6)$$

where $\phi(\gamma_a|\,\bar{\gamma}_a)$ is the probability density function of an exponential distribution with mean $\bar{\gamma}_a$. In all cases, we used the average length of protein-coding exons or CNEs, 152.0 and 50.0 respectively, as τ when fitting equation 4. We assumed that N_e = 426,200, based on $4N_e\mu$ = 0.0092 and a mutation rate of 5.4 x 10^{-9} (Uchimura et al. 2015).

We used our estimates of positive selection parameters to quantify the relative contributions of positive selection in protein-coding exons versus CNEs to the change in population mean fitness. To obtain confidence intervals around our estimates of the ratio of fitness contributed by positive selection in exons versus CNEs ($\Delta W_{Exons}/\Delta W_{CNEs}$), we used a parametric bootstrap approach. For each estimated γ_a and p_a parameter, we sampled random values from a truncated normal distribution with mean equal to the parameter estimate and variance equal to the square of the standard error of the parameter estimate. The truncated normal distribution had a lower bound of 0.0, since values of γ_a and p_a below 0 are biologically impossible. For the calculation of $\Delta W_{Exons}/\Delta W_{CNEs}$, we performed 1,000 bootstraps and used them to estimate 95% confidence intervals.

Data availability

Scripts and code to reproduce all analyses, simulations and figures shown in this study are available at https://github.com/TBooker/MuridRodentProject.

Author Contributions

TRB, BC and PDK devised the study. TRB, BCJ, RJC analysed the data. TRB wrote the first draft of the manuscript. All authors contributed to the writing and editing of the manuscript.

Acknowledgements

We would like to extend thanks to Rosina Savisaar for help with identifying exonic splice enhancers and to Peter Ralph for help with PySlim. We would also like to thank Sally Otto, Michael Whitlock, Nathaniel Sharp and Armando Geraldes for helpful discussions, and especially Dan Halligan for help and guidance throughout the course of this and the preceding projects. This project has received funding from the European Research Council under the European Union's Horizon 2020 research and innovation programme (grant agreement no. 694212).

References

Barton, N. H. (2000). Genetic hitchhiking. *Philos Trans R Soc Lond B Biol Sci*, *355*(1403), 1553–1562. https://doi.org/10.1098/rstb.2000.0716

Booker, T R, Ness, R. W., & Keightley, P. D. (2017). The recombination landscape in wild house mice inferred using population genomic data. *Genetics*, *207*(1), 297–309. https://doi.org/10.1534/genetics.117.300063

Booker, Tom R. (2020). Inferring Parameters of the Distribution of Fitness Effects of New Mutations When Beneficial Mutations Are Strongly Advantageous and Rare. *G3*, *10*(7), 2317–2326. https://doi.org/10.1534/g3.120.401052

Booker, Tom R, & Keightley, P. D. (2018). Understanding the Factors That Shape Patterns of Nucleotide Diversity in the House Mouse Genome. *Molecular Biology and Evolution*, *35*(12), 2971–2988.

Campos, J L, Zhao, L., & Charlesworth, B. (2017). Estimating the parameters of background selection and selective sweeps in Drosophila in the presence of gene conversion. *Proceedings of the National Academy of Sciences*, *114*(24), E4762–E4771. https://doi.org/10.1073/pnas.1619434114 10.5061/dryad.vs264)

Campos, José Luis, & Charlesworth, B. (2019). The effects on neutral variability of recurrent selective sweeps and background selection. *Genetics*, *212*(1), 287–303. https://doi.org/10.1534/genetics.119.301951

Carroll, S. B. (2005). Evolution at two levels: on genes and form. *PLoS Biology*, *3*(7), e245. https://doi.org/10.1371/journal.pbio.0030245

Chan, A. H., Jenkins, P. A., & Song, Y. S. (2012). Genome-wide fine-scale recombination rate variation in Drosophila melanogaster. *PLoS Genetics*, *8*(12), e1003090. https://doi.org/10.1371/journal.pgen.1003090

Charlesworth, B, & Charlesworth, D. (2010). *Elements of Evolutionary Genetics*. Roberts \& Company.

Charlesworth, Brian. (2012). The effects of deleterious mutations on evolution at linked sites. *Genetics*, *190*(1), 5–22. https://doi.org/10.1534/genetics.111.134288

Charlesworth, Brian. (2020). How good are predictions of the effects of selective sweeps on levels of neutral diversity? *Genetics*, *216*(4), 1217–1238. https://doi.org/10.1534/genetics.120.303734

Clark, A. G., Wang, X., & Matise, T. (2010). Contrasting Methods of Quantifying Fine Structure of

Human Recombination. *Annual Review of Genomics and Human Genetics*, *11*(1), 45–64. https://doi.org/10.1146/annurev-genom-082908-150031

Comeron, J. (2014). Background selection as a baseline for nucleotide variation across the Drosophila genome. *PLoS Genetics*, *10*(6). https://doi.org/10.1371/

Cox, A., Ackert-Bicknell, C. L., Dumont, B. L., Ding, Y., Bell, J. T., Brockmann, G. A., Wergedal, J. E., Bult, C., Paigen, B., Flint, J., Tsaih, S. W., Churchill, G. A., & Broman, K. W. (2009). A new standard genetic map for the laboratory mouse. *Genetics*, *182*(4), 1335–1344. https://doi.org/10.1534/genetics.109.105486

Delaneau, O., Howie, B., Cox, A. J., Zagury, J. F., & Marchini, J. (2013). Haplotype estimation using sequencing reads. *Am J Hum Genet*, *93*(4), 687–696. https://doi.org/10.1016/j.ajhg.2013.09.002

Dumont, B. L., & Payseur, B. A. (2011). Genetic analysis of genomic-scale recombiantion rate evolution in house mice. *PLoS Genetics*, *7*(6), 11. https://doi.org/10.1371/

Elyashiv, E., Sattath, S., Hu, T. T., Strutsovsky, A., McVicker, G., Andolfatto, P., Coop, G., & Sella, G. (2016). A genomic map of the effects of linked selection in Drosophila. *PLoS Genetics*, *12*(8), e1006130. https://doi.org/10.1371/journal.pgen.1006130

Enard, D., Messer, P. W., & Petrov, D. A. (2014). Genome-wide signals of positive selection in human evolution. *Genome Research*, *24*(6), 885–895. https://doi.org/10.1101/gr.164822.113

Ewing, G. B., & Jensen, J. D. (2016). The consequences of not accounting for background selection in demographic inference. *Molecular Ecology*, *25*(1), 135–141. https://doi.org/10.1111/mec.13390

Falconer, D. S., & Mackay, T. F. C. (1996). *Introduction to Quantitative Genetics (Fourth Edition)* (Fourth). Pearson Education Limited.

Fisher, R. A. (1918). The Correlation Between Relatives on the Supposition of Mendelian Inheritance. *Transactions of the Royal Society of Edinburgh*, *52*, 399–433.

Gaffney, D. J., & Keightley, P. D. (2008). Effect of the assignment of ancestral CpG state on the estimation of nucleotide substitution rates in mammals. *BMC Evol Biol*, *8*, 265. https://doi.org/10.1186/1471-2148-8-265

Garud, N. R., Messer, P. W., Buzbas, E. O., & Petrov, D. A. (2015). Recent selective sweeps in North American Drosophila melanogaster show signatures of soft sweeps. *PLoS Genetics*, *11*(2), e1005004. https://doi.org/10.1371/journal.pgen.1005004

Garud, N. R., & Petrov, D. A. (2016). Elevated linkage disequilibrium and signatures of soft sweeps are common in Drosophila melanogaster. *Genetics*, *203*(2), 863–880.

https://doi.org/10.1534/genetics.115.184002

Geraldes, A., Basset, P., Smith, K. L., & Nachman, M. W. (2011). Higher differentiation among subspecies of the house mouse (Mus musculus) in genomic regions with low recombination. *Molecular Ecology*, *20*(22), 4722–4736. https://doi.org/10.1111/j.1365-294X.2011.05285.x

Good, B. H., Walczak, A. M., Neher, R. A., & Desai, M. M. (2014). Genetic Diversity in the Interference Selection Limit. *PLoS Genetics*, *10*(3). https://doi.org/10.1371/journal.pgen.1004222

Gordo, I., Navarro, A., & Charlesworth, B. (2002). Muller's Ratchet and the Pattern of Variation at a Neutral Locus. *Genetics*, *161*, 835–848.

Haldane, J. B. S. (1927). A Mathematical Theory of Natural and Artificial Selection, Part V: Selection and Mutation. *Mathematical Proceedings of the Cambridge Philosophical Society*, *23*(7), 838–844. https://doi.org/10.1017/S0305004100015644

Haller, B. C., & Messer, P. W. (2019). SLiM 3: Forward Genetic Simulations Beyond the Wright-Fisher Model. *Molecular Biology and Evolution*, *36*(3), 632–637.

Halligan, D. L., Kousathanas, A., Ness, R. W., Harr, B., Eory, L., Keane, T. M., Adams, D. J., & Keightley, P. D. (2013). Contributions of protein-coding and regulatory change to adaptive molecular evolution in murid rodents. *PLoS Genetics*, *9*(12), e1003995. https://doi.org/10.1371/journal.pgen.1003995

Halligan, D. L., Oliver, F., Eyre-Walker, A., Harr, B., & Keightley, P. D. (2010). Evidence for pervasive adaptive protein evolution in wild mice. *PLoS Genetics*, *6*(1), e1000825. https://doi.org/10.1371/journal.pgen.1000825

Harr, B., Karakoc, E., Neme, R., Teschke, M., Pfeifle, C., Pezer, Ž., Babiker, H., Linnenbrink, M., Montero, I., Scavetta, R., Abai, M. R., Molins, M. P., Schlegel, M., Ulrich, R. G., Altmüller, J., Franitza, M., Büntge, A., Künzel, S., & Tautz, D. (2016). Genomic resources for wild populations of the house mouse, Mus musculus and its close relative Mus spretus. *Scientific Data*, *3*. https://doi.org/10.1038/sdata.2016.75

Harris, R. B., Sackman, A., & Jensen, J. D. (2018). On the unfounded enthusiasm for soft selective sweeps II: Examining recent evidence from humans, flies, and viruses. *PLoS Genetics*, *14*(12), e1007859. https://doi.org/10.1371/journal.pgen.1007859

Hermisson, J., & Pennings, P. S. (2017). Soft sweeps and beyond: understanding the patterns and probabilities of selection footprints under rapid adaptation. *Methods in Ecology and Evolution*, *8*(6), 700–716. https://doi.org/10.1111/2041-210x.12808

Hernandez, R. D., Kelly, J. L., Elyashiv, E., Melton, S. C., Auton, A., McVean, G., Project, 1000

Genomes, Sella, G., & Przeworski, M. (2011). Classic selective sweeps were rare in recent human evolution. *Science*, *331*, 920–924.

Hoekstra, H. E., & Coyne, J. A. (2007). The locus of evolution: Evo devo and the genetics of adaptation. *Evolution*, *61*(5), 995–1016. https://doi.org/10.1111/j.1558-5646.2007.00105.x

Howe, K. L., Achuthan, P., Allen, J., Allen, J., Alvarez-Jarreta, J., Ridwan Amode, M., Armean, I. M., Azov, A. G., Bennett, R., Bhai, J., Billis, K., Boddu, S., Charkhchi, M., Cummins, C., da Rin Fioretto, L., Davidson, C., Dodiya, K., El Houdaigui, B., Fatima, R., … Flicek, P. (2021). Ensembl 2021. *Nucleic Acids Research*, *49*(D1), D884–D891. https://doi.org/10.1093/nar/gkaa942

Jain, K., & Stephan, W. (2017). Rapid adaptation of a polygenic trait after a sudden environmental shift. *Genetics*, *206*(1), 389–406.

Johri, P., Riall, K., Becher, H., Excoffier, L., Charlesworth, B., & Jensen, J. D. (2021). The Impact of Purifying and Background Selection on the Inference of Population History: Problems and Prospects. *Molecular Biology and Evolution*. https://doi.org/10.1093/molbev/msab050

Keightley, P. D., & Jackson, B. C. (2018). Inferring the Probability of the Derived vs. the Ancestral Allelic State at a Polymorphic Site. *Genetics*, *209*(3), 897–906.

Kern, A. D., & Hahn, M. W. (2018). The neutral theory in light of natural selection. *Molecular Biology and Evolution*, *35*(6), 1366–1371. https://doi.org/10.1093/molbev/msy092

Kim, Y., & Stephan, W. (2000). Joint effects of genetic hitchhiking and background selection on neutral variation. *Genetics*, *155*, 1415–1427.

Kimura, M., & Ohta, T. (1971). *Theoretical aspects of population genetics*. Princeton Univ. Press.

King, M.-C., & Wilson, A. C. (1975). Evolution at two levels in humans and chimpanzees. *Science*, *188*(4184), 107–116.

Kousathanas, A., & Keightley, P. D. (2013). A comparison of models to infer the distribution of fitness effects of new mutations. *Genetics*, *193*(4), 1197–1208. https://doi.org/10.1534/genetics.112.148023

Lawal, R. A., Arora, U. P., & Dumont, B. L. (2021). Selection shapes the landscape of functional variation in wild house mice 1 2. *BioRxiv*, 2021.05.12.443838. https://doi.org/10.1101/2021.05.12.443838

Leffler, E. M., Bullaughey, K., Matute, D. R., Meyer, W. K., Segurel, L., Venkat, A., Andolfatto, P., & Przeworski, M. (2012). Revisiting an old riddle: what determines genetic diversity levels within species? *PLoS Biology*, *10*(9), e1001388. https://doi.org/10.1371/journal.pbio.1001388

Li, H. (2013). *Aligning sequence reads, clone sequences and assembly contigs with BWA-MEM*. http://arxiv.org/abs/1303.3997

1000 Lindblad-Toh, K., Garber, M., Zuk, O., Lin, M. F., Parker, B. J., Washietl, S., Kheradpour, P., Ernst, J.,
1001 Jordan, G., Mauceli, E., Ward, L. D., Lowe, C. B., Holloway, A. K., Clamp, M., Gnerre, S., Alföldi,
1002 J., Beal, K., Chang, J., Clawson, H., … Sodergren, E. (2011). A high-resolution map of human
1003 evolutionary constraint using 29 mammals. *Nature*, *478*(7370), 476–482.
1004 https://doi.org/10.1038/nature10530
1005 Lowe, C. B., Kellis, M., Siepel, A., Raney, B. J., Clamp, M., Salama, S. R., Kingsley, D. M., Lindblad-
1006 Toh, K., & Haussler, D. (2011). Three periods of regulatory innovation during vertebrate
1007 evolution. *Science*, *333*(6045), 1019–1024. https://doi.org/10.1126/science.1202702
1008 Lynch, M., Bürger, R., Butcher, D., & Gabriel, W. (1993). The Mutational Meltdown in Asexual
1009 Populations. *Journal of Heredity*, *84*(5), 339–344.
1010 https://doi.org/10.1093/oxfordjournals.jhered.a111354
1011 McKenna, A., Hanna, M., Banks, E., Sivachenko, A., Cibulskis, K., Kernytsky, A., Garimella, K.,
1012 Altshuler, D., Gabriel, S., Daly, M., & DePristo, M. A. (2010). The genome analysis toolkit: A
1013 MapReduce framework for analyzing next-generation DNA sequencing data. *Genome*
1014 *Research*, *20*(9), 1297–1303. https://doi.org/10.1101/gr.107524.110
1015 McVicker, G., Gordon, D., Davis, C., & Green, P. (2009). Widespread genomic signatures of natural
1016 selection in hominid evolution. *PLoS Genetics*, *5*(5), e1000471.
1017 https://doi.org/10.1371/journal.pgen.1000471
1018 Mikkelsen, T. S., Wakefield, M. J., Aken, B., Amemiya, C. T., Chang, J. L., Duke, S., Garber, M.,
1019 Gentles, A. J., Goodstadt, L., Heger, A., Jurka, J., Kamal, M., Mauceli, E., Searle, S. M. J.,
1020 Sharpe, T., Baker, M. L., Batzer, M. A., Benos, P. V., Belov, K., … Lindblad-Toh, K. (2007).
1021 Genome of the marsupial Monodelphis domestica reveals innovation in non-coding
1022 sequences. *Nature*, *447*(7141), 167–177. https://doi.org/10.1038/nature05805
1023 Obbard, D. J., Welch, J. J., Kim, K. W., & Jiggins, F. M. (2009). Quantifying adaptive evolution in the
1024 Drosophila immune system. *PLoS Genetics*, *5*(10), 1000698.
1025 https://doi.org/10.1371/journal.pgen.1000698
1026 Paigen, K., Szatkiewicz, J. P., Sawyer, K., Leahy, N., Parvanov, E. D., Ng, S. H., Graber, J. H., Broman,
1027 K. W., & Petkov, P. M. (2008). The recombinational anatomy of a mouse chromosome. *PLoS*
1028 *Genetics*, *4*(7), e1000119. https://doi.org/10.1371/journal.pgen.1000119
1029 Pouyet, F., Aeschbacher, S., Thiéry, A., & Excoffier, L. (2018). Background selection and biased
1030 gene conversion affect more than 95% of the human genome and bias demographic
1031 inferences. *ELife*, *7*. https://doi.org/10.7554/eLife.36317
1032 Pritchard, J. K., Pickrell, J. K., & Coop, G. (2010). The genetics of human adaptation: hard sweeps,

1033 soft sweeps, and polygenic adaptation. *Current Biology*, *20*(4), R208-15.
1034 https://doi.org/10.1016/j.cub.2009.11.055
1035 Santiago, E., & Caballero, A. (2005). Variation after a selective sweep in a subdivided population.
1036 *Genetics*, *169*(1), 475–483. https://doi.org/10.1534/genetics.104.032813
1037 Sattath, S., Elyashiv, E., Kolodny, O., Rinott, Y., & Sella, G. (2011). Pervasive adaptive protein
1038 evolution apparent in diversity patterns around amino acid substitutions in Drosophila
1039 simulans. *PLoS Genetics*, *7*(2), e1001302. https://doi.org/10.1371/journal.pgen.1001302
1040 Savisaar, R., & Hurst, L. D. (2018). Exonic splice regulation imposes strong selection at synonymous
1041 sites. *Genome Research*, *28*(10), 1442–1454. https://doi.org/10.1101/gr.233999.117
1042 Schrider, D. R., & Kern, A. D. (2016). S/HIC: Robust Identification of Soft and Hard Sweeps Using
1043 Machine Learning. *PLoS Genetics*, *12*(3), e1005928.
1044 https://doi.org/10.1371/journal.pgen.1005928
1045 Siepel, A., Bejerano, G., Pedersen, J. S., Hinrichs, A. S., Hou, M., Rosenbloom, K., Clawson, H.,
1046 Spieth, J., Hillier, L. D. W., Richards, S., Weinstock, G. M., Wilson, R. K., Gibbs, R. A., Kent, W.
1047 J., Miller, W., & Haussler, D. (2005). Evolutionarily conserved elements in vertebrate, insect,
1048 worm, and yeast genomes. *Genome Research*, *15*(8), 1034–1050.
1049 https://doi.org/10.1101/gr.3715005
1050 Simonsen, K. L., Churchill, G. A., & Aquadro, C. F. (1995). Properties of statistical tests of neutrality
1051 for DNA polymorphism data. *Genetics*, *141*(1).
1052 Stephan, W. (2019). Selective sweeps. *Genetics*, *211*(1), 5–13.
1053 https://doi.org/10.1534/genetics.118.301319
1054 Stern, D. L., & Orgogozo, V. (2008). The loci of evolution: How predictable is genetic evolution?
1055 *Evolution*, *62*(9), 2155–2177. https://doi.org/10.1111/j.1558-5646.2008.00450.x
1056 Tataru, P., & Bataillon, T. (2019). polyDFEv2.0: testing for invariance of the distribution of fitness
1057 effects within and across species. *Bioinformatics*, *35*(16), 2868–2869.
1058 https://doi.org/10.1093/bioinformatics/bty1060
1059 Tataru, P., Mollion, M., Glemin, S., & Bataillon, T. (2017). Inference of distribution of fitness effects
1060 and proportion of adaptive substitutions from polymorphism data. *Genetics*, *207*(3), 1103–
1061 1119. https://doi.org/10.1534/genetics.117.300323
1062 Teschke, M., Mukabayire, O., Wiehe, T., & Tautz, D. (2008). Identification of selective sweeps in
1063 closely related populations of the house mouse based on microsatellite scans. *Genetics*, *180*,
1064 1537–1545.
1065 Thybert, D., Roller, M., Navarro, F. C. P., Fiddes, I., Streeter, I., Feig, C., Martin-Galvez, D.,

1066 Kolmogorov, M., Janoušek, V., Akanni, W., Aken, B., Aldridge, S., Chakrapani, V., Chow, W.,
1067 Clarke, L., Cummins, C., Doran, A., Dunn, M., Goodstadt, L., … Flicek, P. (2018). Repeat
1068 associated mechanisms of genome evolution and function revealed by the Mus caroli and
1069 Mus pahari genomes. *Genome Research*, *28*(4), 448–459.
1070 https://doi.org/10.1101/gr.234096.117
1071 Torres, R., Stetter, M. G., Hernandez, R. D., & Ross-Ibarra, J. (2020). The Temporal Dynamics of
1072 Background Selection in Nonequilibrium Populations. *Genetics*, *214*(4), 1019–1030.
1073 https://doi.org/10.1534/genetics.119.302892
1074 Uchimura, A., Higuchi, M., Minakuchi, Y., Ohno, M., Toyoda, A., Fujiyama, A., Miura, I., Wakana, S.,
1075 Nishino, J., & Yagi, T. (2015). Germline mutation rates and the long-term phenotypic effects
1076 of mutation accumulation in wild-type laboratory mice and mutator mice. *Genome Research*,
1077 *25*(8), 1125–1134. https://doi.org/10.1101/gr.186148.114
1078 Wiehe, T., & Stephan, W. (1993). Analysis of a genetic hitchhiking model, and its application to
1079 DNA polymorphism data from Drosophila melanogaster. *Molecular Biology and Evolution*,
1080 *10*(4), 842–854.
1081 Williamson, R. J., Josephs, E. B., Platts, A. E., Hazzouri, K. M., Haudry, A., Blanchette, M., & Wright,
1082 S. I. (2014). Evidence for widespread positive and negative selection in coding and conserved
1083 noncoding regions of Capsella grandiflora. *PLoS Genetics*, *10*(9), e1004622.
1084 https://doi.org/10.1371/journal.pgen.1004622
1085 Wray, G. A. (2007). The evolutionary significance of cis-regulatory mutations. *Nature Reviews*
1086 *Genetics*, *8*(3), 206–216. https://doi.org/10.1038/nrg2063
1087

1088

Supplementary Material

Appendix: Analyses assuming LD-based recombination maps

Generating LD-based recombination rate maps

We phased variant calls using the read-aware methodology incorporated in SHAPEIT2 (Delaneau et al., 2013). For each of the mouse population samples, we carried out the following procedure. First, we created a stringently filtered set of SNPs following Booker et al. (2017), by only including biallelic variant sites that met the following criteria: no overlap with indels, no missing data, QUAL >= 30, genotype quality (GQ) greater than or equal to 15 in all individual genotypes, sequencing depth (DP) greater than or equal to 10 for all individuals, rejected sites with significant deviation from Hardy-Weinberg equilibrium at the level $p < 0.05$). Using the filtered variants, we extracted phase informative reads. We then ran SHAPEIT2 in 'assemble' mode to phase our stringently filtered variants. Finally, we converted the output of SHAPEIT2 to FASTA files, which contained two haplotypes per diploid sample using custom Python scripts.

We ran LDhelmet version 1.9 (Chan et al. 2012) on the phased haplotypes, in order to estimate the population-scaled recombination rate, $\rho = 4N_e r$, where N_e is the effective population size and r is the rate of crossing over between two sites per generation, for each of the mouse populations. We calculated the ancestral prior probability for each variant site that we passed to LDhelmet using the method developed by Keightley & Jackson (2018) as implemented in the program *est-sfs* v2.01. As input for this program, we generated files including each variant and invariant site that met less stringent filtering criteria than that described above (QUAL > 30, no missing data, no overlap with indels, ExcessHet < 13, no more than two alleles per site), and additionally discarded sites that did not have full outgroup information (alleles from both *Mus famulus* and *Mus pahari* for mouse samples mapped to mm10). For sites that were present in the input to LDhelmet, but not in the input for the Keightley & Jackson (2018) method, because they lacked complete outgroup data, we assigned the ancestral prior following Equation 18 in Keightley & Jackson (2018). We used the resulting information about the ancestral states of SNPs to populate the 4x4

1118 mutation transition matrix used by LDhelmet (Chan et al. 2012). To estimate fine-scale
1119 recombination rates in each of our populations, we ran the *find_confs* component of LDhelmet
1120 with a window size (-w) of 50 SNPs to generate haplotype configuration files from the phased
1121 FASTA files we made in the step above. Subsequently, we ran the *table_gen* and *pade* components
1122 of LDhelmet with the default parameters, with the exception of θ [-t] which we set to the point
1123 estimate of π at 4-fold degenerate synonymous sites specific to each population. To estimate ρ we
1124 ran the *rjmcmc* component of LDhelmet with a width [-w] of 50 SNPs, a block penalty [-b] of 100, a
1125 partition length of 4001 SNPs, an overlap of 200 SNPs, a burn-in period of 100,000 iterations
1126 followed by 1,000,000 iterations of the Markov chain.
1127

1128 ### Comparison of LD-based recombination rates among taxa

1129 When analysing patterns of genetic diversity under a model of selection at linked sites, the way in
1130 which recombination rate estimates were obtained may affect parameter estimates. We analysed
1131 the relationship between nucleotide diversity and genetic distance from functional elements in *M.*
1132 *m. castaneus* assuming either a high-resolution recombination map constructed using patterns of
1133 linkage disequilibrium (LD) or the pedigree-based map constructed by Cox et al. (2009). These two
1134 approaches for generating recombination rate maps have both advantages and disadvantages. By
1135 examining patterns of LD, the population-scaled recombination rate ($\rho = 4N_e r$), where r is the
1136 recombination rate, can be inferred from a relatively small sample of unrelated individuals at very
1137 fine-scales. However, natural selection can influence LD and may therefore affect such
1138 recombination rate estimates (Clark et al. 2010). Alternatively, direct estimates of the
1139 recombination rate can be obtained from crossing experiments, but to achieve a high-resolution
1140 recombination map, a very large number of individuals need to be genotyped and this has typically
1141 precluded the use of whole-genome re-sequencing in some species such as mice, thereby limiting
1142 resolution.
1143

1144 We generated recombination rate maps from patterns of LD for each of the mouse taxa, and
1145 compared these to the pedigree-based estimates obtained by Cox et al. (2009). It is worth pointing
1146 out that the Cox et al. (2009) map is an estimate of the recombination map that was generated
1147 using inbred strains of mice of predominantly *M. m. domesticus* origin and there are known
1148 differences in total genetic map length and local recombination rate between *M. musculus* sub-
1149 species (Dumont & Payseur 2011). For simplicity, we treat the Cox map as a baseline comparison
1150 for each of the recombination rate landscapes we inferred.

We calculated Spearman's correlation between LD-based recombination rate estimates obtained for each mouse taxa and recombination rate estimates from the Cox map in windows from 1Mbp up to 20Mbp. Across all scales tested, the recombination maps for *M. m. castaneus* and *M. m. musculus* from Afghanistan showed the highest level of congruence with the Cox map (Figure A.1). The correlation exhibited by the *M. m. castaneus* was very similar to the correlation previously reported (Booker et al., 2017). For the purposes of calculating genetic distances, we used the LD-based recombination rate estimates for *M. m. castaneus*.

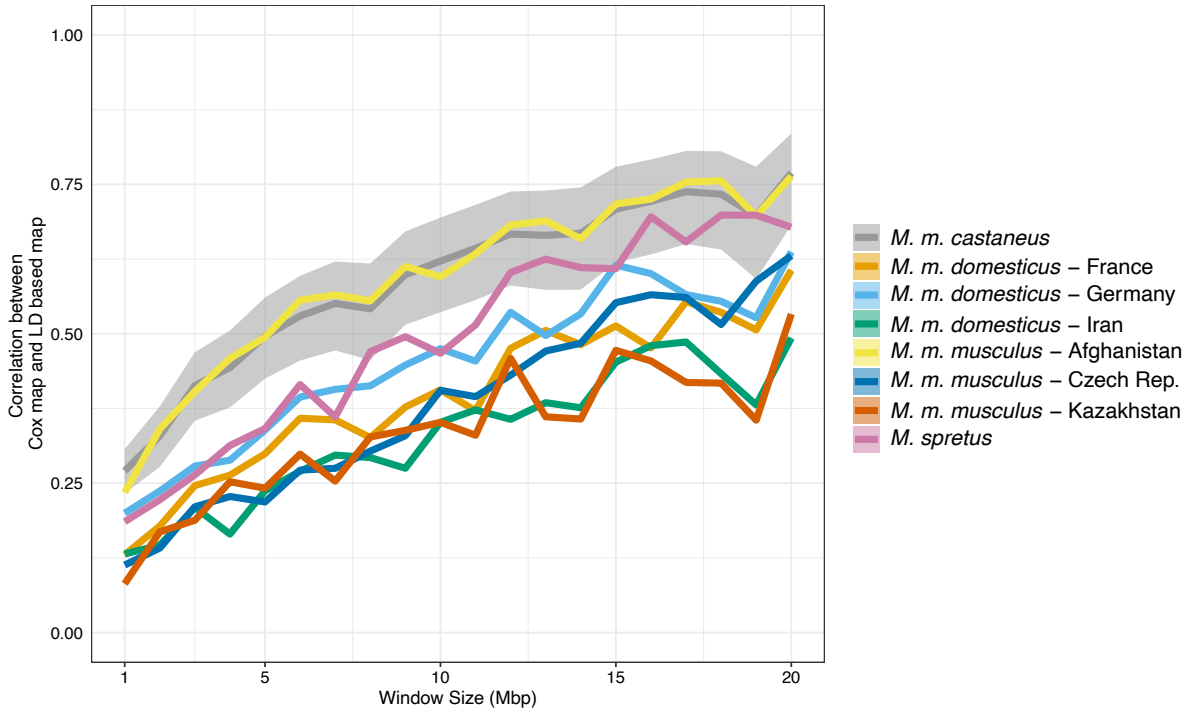

Figure A.1 Spearman rank correlation coefficients between recombination maps inferred using LDhelmet for wild mice and the pedigree-based map of Cox et al. (2009). Correlations were calculated in non-overlapping windows of discrete physical size. For the purposes of visualisation, the confidence interval is only shown for the *M. m castaneus* map.

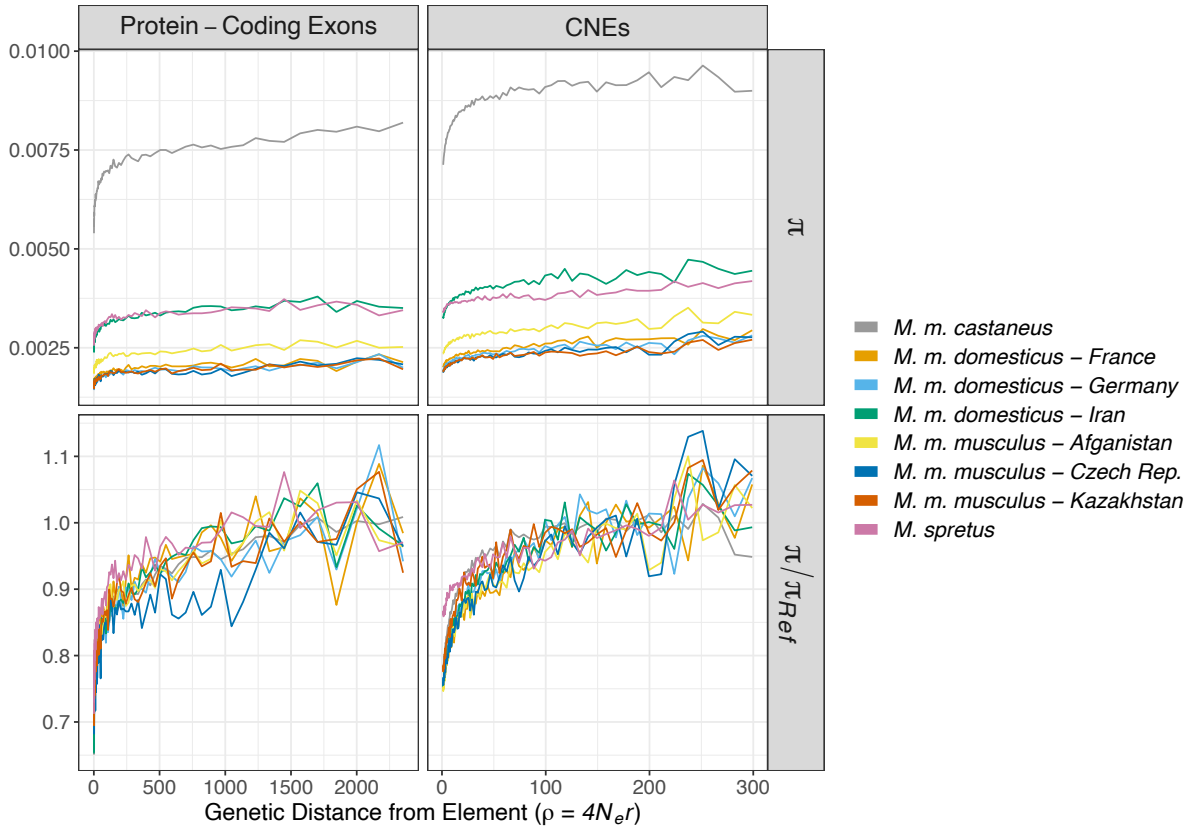

Figure A.2 Identical to Figure 2 in the main text except that genetic distances were calculated assuming the LD-based recombination map constructed for *M. m. castaneus*.

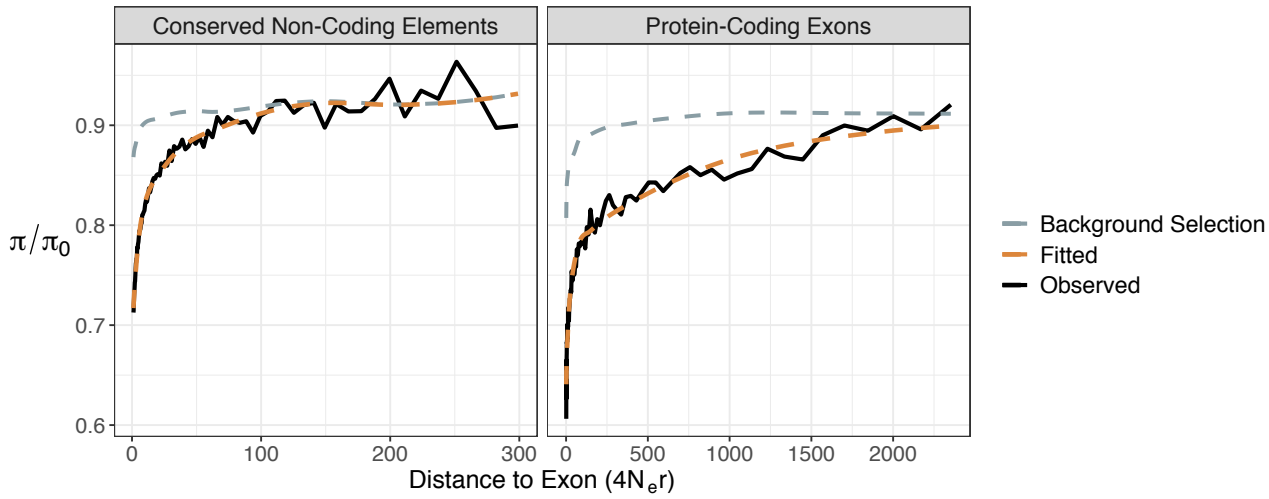

Supplementary Table S1 Comparison of uSFS model fits for each taxa and class of sites considered. The maximum likelihood estimate of model parameters are shown along with the estimated uSFS. A parameter key is given as a second sheet in the spreadsheet.

1176 **Supplementary Table S2** Parameters of the distribution of fitness effects for deleterious mutations
1177 as well as the positive selection parameters estimated for each population using *polyDFE*. Point
1178 estimates are provided as well as 95% bootstrap confidence intervals. A parameter key is given as
1179 an additional sheet in the spreadsheet.
1180
1181 **Supplementary Table S3** Estimates of positive selection parameters obtained by fitting a models
1182 of selective sweeps and background selection to troughs in nucleotide diversity. Parameters are
1183 given for models assuming a one or two discrete classes of advantageous mutations as well as an
1184 exponential distribution of fitness effects. Estimates of the fitness change brought about by
1185 positive selection in protein-coding exons and CNEs are also given in the table. A parameter key is
1186 given as an additional sheet in the spreadsheet.
1187

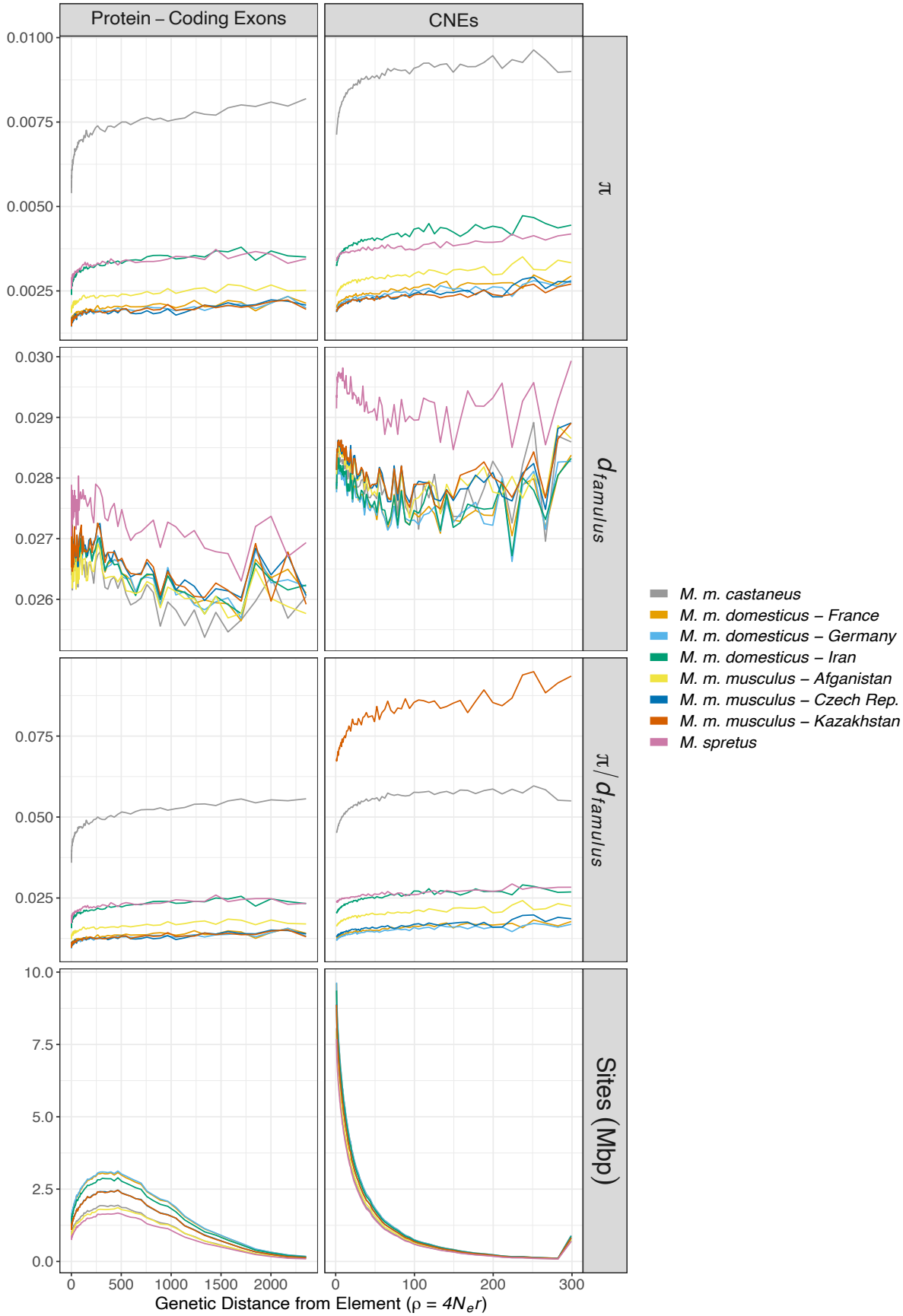

Figure S1 Additional summary statistics in the regions surrounding functional elements assuming the LD-based map of recombination rate variation we inferred for *M. m. castaneus.*

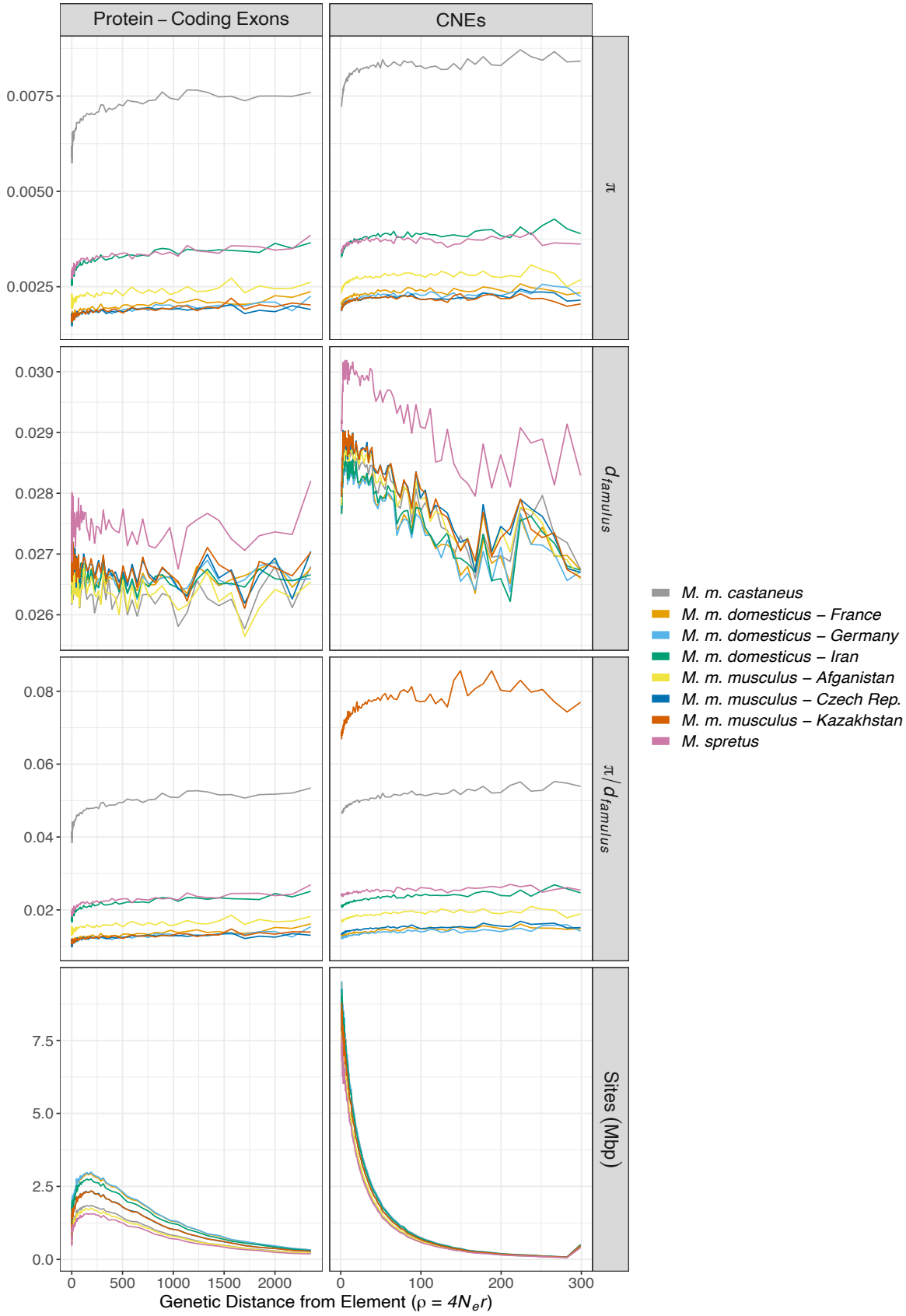

Figure S2 Additional summary statistics in the regions flanking functional elements assuming the Cox map.

1195

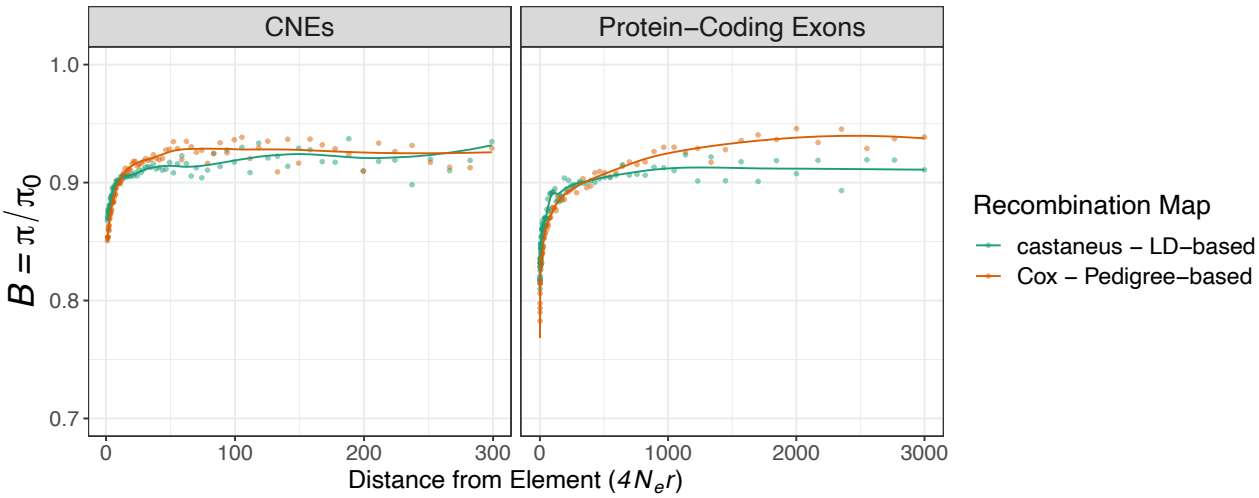

1196

1197 **Figure S3** The reduction in neutral genetic diversity relative to neutral expectation caused by
1198 background selection (*B*) observed in simulated datasets. Simulations assumed either the LD-
1199 based recombination map or the pedigree-based map of Cox et al. (2009). Lines indicate the fit of
1200 a Loess regression fitted to the data with a span of 0.3 and the number of sites in each bin used as
1201 weights.

1202

1203

1204

1205

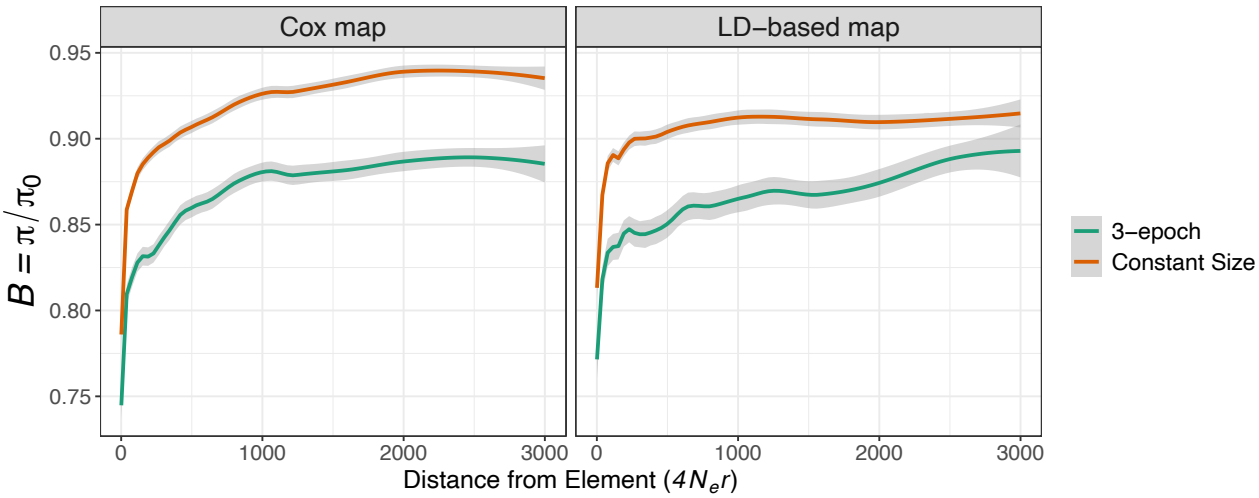

1206

1207 **Figure S4** The reductions in neutral genetic diversity relative to neutral expectation caused by
1208 background selection (*B*) observed in simulated datasets when modelling a population with
1209 constant size, or the three-epoch demographic model estimated by Booker and Keightley (2018).
1210 π_0 in the constant size simulations was 0.01. π_0 was 0.0042 in the 3-epoch simulations, which was
1211 calculated from the harmonic mean of population sizes. Lines indicate the fit of a Loess regression
1212 fitted to the data.

1213

1214